Geomorphology 381 (2021) 107648

Contents lists available at ScienceDirect

Geomorphology

journal homepage: www.elsevier.com/locate/geomorph

The effect of global warming on the establishment of mangroves in coastal Louisiana during the Holocene

Erika Rodrigues [a], Marcelo C.L. Cohen [a,*], Kam-biu Liu [b], Luiz C.R. Pessenda [c], Qiang Yao [b], Junghyung Ryu [b], Dilce Rossetti [d], Adriana de Souza [a], Marianne Dietz [b]

[a] Laboratory of Coastal Dynamics, Graduate Program of Geology and Geochemistry, Federal University of Pará, Brazil Federal University of Pará, Rua Augusto Corrêa, 01 - Guamá, CEP 66075-110 Belém, PA, Brazil
[b] Department of Oceanography and Coastal Sciences, Louisiana State University, Baton Rouge, LA 70803, USA
[c] University of São Paulo, CENA/^{14}C Laboratory, Av. Centenário 303, 13400-000 Piracicaba, São Paulo, Brazil
[d] National Space Research Institute (INPE), Rua dos Astronautas 1758-CP 515, CEP: 12245-970 São José dos Campos, SP, Brazil

ARTICLE INFO

Article history:
Received 15 July 2020
Received in revised form 26 January 2021
Accepted 28 January 2021
Available online 10 February 2021

Keywords:
Anthropocene
Avicennia
Isotopes
Palynology
Port Fourchon

ABSTRACT

Winter temperature and sea-level position are critical factors affecting the global distribution of mangroves and saltmarshes. The replacement of saltmarshes by mangroves is expected due to global warming, reflecting the long-term natural trends in the Holocene and anthropogenic impacts since the 20th century. We documented the Holocene history of wetlands dynamics in the boreal limits of the American mangroves, located at Bay Champagne, Louisiana (USA), by integrating sedimentological, palynological, geochemical (δ^{13}C and C\N), X-ray fluorescence (XRF) data, and radiocarbon chronology from two sediment cores. The results indicated a freshwater lake environment with herbs and wetland ferns, as well as C_3 terrestrial plants, between ~8100 and ~6500 cal yr BP. This environment shifted into a lagoon and saltmarshes having sedimentary organic matter sourced from marine algae between ~6500 and ~1500 cal yr BP. In the final stage, washover sediments were deposited in the lagoon during the last ~1500 cal yr BP. Despite the increased marine influence over the last ~6500 cal yr BP, mangrove pollen were not recorded between ~8100 and ~1500 cal yr BP, suggesting that mangroves were absent in the study area during that time interval. Historical evidence and a comparative analysis of our multi-proxy data with other mangrove studies from the Gulf of Mexico, Caribbean, and eastern South America revealed a gradual mangrove expansion from tropical to subtropical coasts of South and North America during the mid-late Holocene. The mangrove colonies at their current boreal (29° 09′ N) and austral (28° 29′ S) limits were established in the early and mid-20th century, respectively. This mangrove dynamics on a continental scale suggests that the poleward mangrove migration was likely caused by the warming climate during the Holocene. More importantly, the industrial-era warming has likely accelerated the mangrove expansion, but it was not the primary force that drove the mangrove migration into temperate zones.

1. Introduction

Mangroves are perhaps some of the most typical ecosystems of tropical coasts, consisting of valuable and productive intertidal forests (Food and Agriculture Organization of the United Nations, 2007; Ribeiro et al., 2019). The main products and services of mangroves include protection from storms and sea-level rise (Alongi, 2008); plant and animal productivity (Ewel et al., 1998); sources of organic matter for coastal ecosystems (Walsh and Nittrouer, 2004; Dittmar et al., 2006); and sequestration and storage of atmospheric and oceanic carbon, thereby mitigating climate change effects (Fisher and Huo, 2012; Taillardat et al., 2018).

Mangroves are also very useful indicators of climate and sea-level changes (Blasco et al., 1996; Fromard et al., 2004; Alongi, 2008) due to the high susceptibility to variations in air/water temperatures, subsidence, tidal flooding frequency, river discharge, estuarine salinity, and nutrient flux, as well as tropical cyclones intensified by climate changes (Amaral et al., 2006; McLeod and Salm, 2006; Cohen et al., 2012; Krauss et al., 2014; Liu et al., 2014; Alongi, 2015; Yao and Liu, 2017). However, depending on the latitude and proximity of large estuaries, some environmental drivers may operate more intensely in controlling the mangrove dynamics, such as winter temperatures on subtropical zones (Cohen et al., 2020b), and fluvial discharge, for instance, near the Amazon River (Cohen et al., 2012). Regarding the northern and southern limits of American mangroves, the air/water temperature becomes the most critical factor in controlling the establishment, expansion, and contraction of mangroves (Cavanaugh et al., 2018, 2019). This ecosystem cannot develop under low temperatures, and then they occur mainly between latitudes 25° N and 25° S (Giri et al., 2011). Its distribution is limited to zones where the coldest-monthly temperature average is above 20 °C and the annual temperature range is <5 °C (Walsh, 1974;

* Corresponding author at: Federal University of Pará - Brazil, Rua Augusto Corrêa, 01 - Guamá, CEP 66075-110 Belém, PA, Brazil.
E-mail address: mcohen@ufpa.br (M.C.L. Cohen).

https://doi.org/10.1016/j.geomorph.2021.107648
0169-555X/

Chapman, 1975; Duke, 1992). This restriction is associated with mangrove's low tolerance to low air temperature, usually inhibiting at around 5 °C (Tomlinsom, 1986; Stuart et al., 2007; Krauss et al., 2014). A consequence of global warming is that mangroves can expand into temperate zones. Some studies have documented the influence of changes in air temperature in the latitudinal distribution of mangroves (Everitt et al., 1996; Stevens et al., 2006; Perry and Mendelssohn, 2009; Stokes et al., 2010; Osland et al., 2015, 2017, 2018, 2019).

Records of mangrove species on Earth during the Tertiary (Sherrod and McMillan, 1985) and Quaternary (Cannon et al., 2009) revealed that the climate controlled their establishment and extinction in the northern hemisphere (Sun and Li, 1999). Mangrove dynamics is generally associated with global climate and sea-level changes since the Last Glacial Maximum (LGM) (Alongi, 2008). In North America, there were alternations of mangrove expansion and contraction in response to pronounced changes in temperatures over the late Quaternary (Sherrod and McMillan, 1985; Woodroffe and Grindrod, 1991; Sandoval-Castro et al., 2012; Saintilan et al., 2014; Osland et al., 2017), and they were restricted to regions equatorward of their modern limits during the LGM. During this period, mangroves also decreased in Asia and Europe (Woodroffe and Grindrod, 1991; Cannon et al., 2009), being restricted to refuge areas with less impact of cold air temperature (Cannon et al., 2009). However, a poleward expansion was recorded in the Northern Hemisphere after 19,000 years ago (Sandoval-Castro et al., 2012; Kennedy et al., 2016). In the Caribbean, mangrove northern limit retreated to more equatorial zones during the Pleistocene (Sherrod and McMillan, 1985). As a result of warmer climates and higher sea levels during the Holocene, mangroves expanded poleward, reaching Florida (Yao and Liu, 2017), Texas (Sherrod and McMillan, 1985), and Louisiana (McKee and Vervaeke, 2018) at different times.

According to pollen and isotopic studies from the South China Sea, mangroves would have replaced boreal forests and temperate grasslands due to a slight increase in air temperature and slow marine transgression at ~14,000 cal yr BP (Sun and Li, 1999). Meanwhile, mangroves were not recorded in North America or Europe, probably due to the low temperatures (Sherrod and McMillan, 1985).

The increased winter temperatures during the last century (IPCC, 2014), mainly in boreal and temperate regions (Solomon et al., 2007), caused a mangrove expansion in the Gulf of Mexico (Cavanaugh et al., 2014), resulting in the replacement of salt marsh vegetation dominated by *Spartina alterniflora* (Sherrod and McMillan, 1985).

The ecological implications of global warming to the new biogeography of ecosystems adapted to tropical areas in the near future can be studied by reconstructing the long-term dynamics of mangroves, mainly along the northern and southern mangrove limits in the Americas. As such, a stratigraphic analysis of mangroves relative to sea-level and climate changes during the Holocene must be provided from various coastal environments to permit an inter-regional comparison. This work aims to discuss the influence of sea-level changes and global warming on American mangroves during the Holocene. We studied the Holocene changes in coastal depositional paleoenvironments, and the dynamics of temperate vegetation and mangroves in southern Louisiana, USA, representing the modern boreal limit of the American mangroves, by the integration of sedimentological, palynological, geochemical ($\delta^{13}C$ and C\N), X-ray fluorescence (XRF) data, and radiocarbon chronology. These data are essential to evaluate and calibrate models that predict the fate of mangroves as the minimum winter temperatures continue to increase (Cavanaugh et al., 2014, 2015, 2018).

2. Study area

2.1. Geomorphology

The Caminada-Moreau Headland is a complex mosaic of barrier islands formed by the transport of sediments by wind, waves, and tidal and longshore currents (Kulp et al., 2005). The study area in Bay

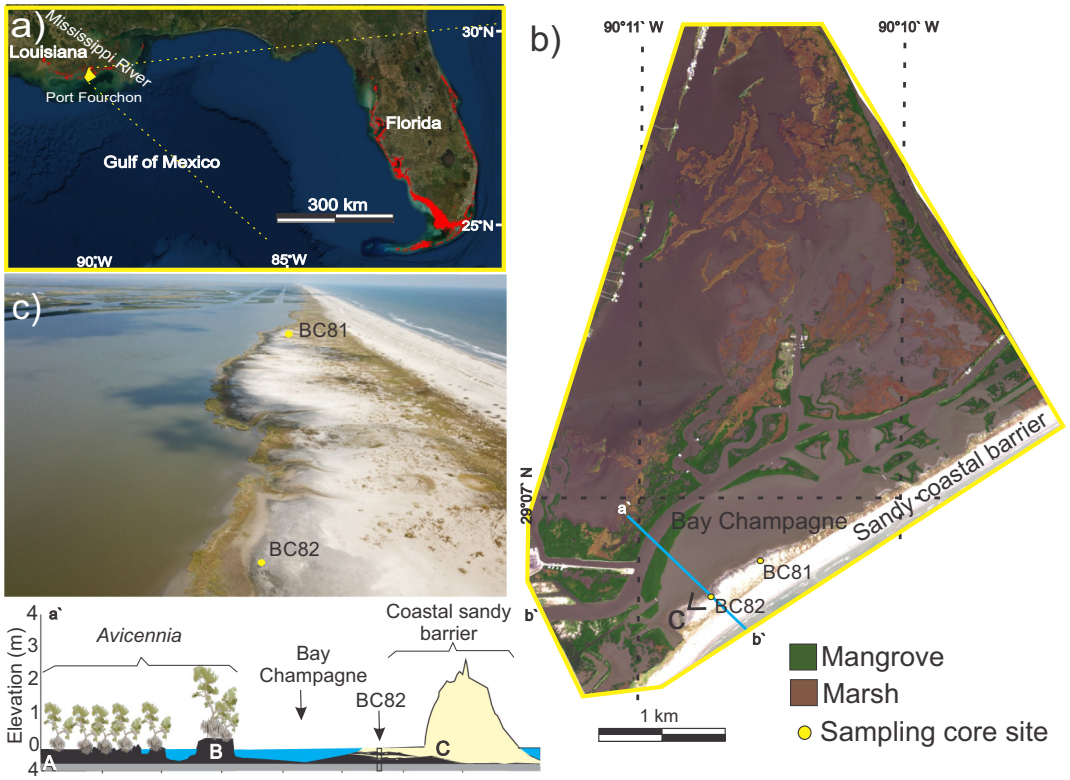

Fig. 1. a) Location of the study area, b) vegetation map with a stratigraphic profile (a′–b′) exhibiting vegetation, geomorphology, and the facies associations, c) drone image showing the coring sites along a sandy coastal barrier.

Champagne (29° 6′ 53, 10″ N/90° 10′ 33, 38″W, Fig. 1) is located in the southwestern end of this headland, near Port Fourchon in the State of Louisiana. This site is part of the Lafourche complex delta lobes, formed ~3500 years ago, and remained active until 1600 to 600 cal yr BP. During this time, nutrient-rich sediments were deposited in floodplains along tributaries, contributing to establishing wetland systems across subdeltas (Blum and Roberts, 2012).

Bay Champagne (BC) is a semi-circular brackish lagoon (salinity: 32‰) (Fig. 1b, and c), with a maximum depth of 2.5 m (Liu et al., 2011). The lagoon is surrounded by cordgrass (*Spartina alterniflora*) and black mangrove (*Avicennia germinans*) vegetation (Naquin et al., 2014). A sandy barrier, standing ~2 m above the mean relative sea-level, partially protects the backbarrier tidal flat wetlands from the impact of high energy waves and storm-forced winds (Dietz et al., 2018). Local barrier islands, including the Timbalier Island and Grand Isle (Shea Penland, 1988), are strongly affected by erosion due to overwashing (Liu et al., 2011; Dietz et al., 2018). In addition, the decadal historical record from Bay Champaign indicates rapid shoreline retreat and coastal erosion in this area, especially during active periods of hurricanes, exacerbating the long-term trend of coastal subsidence and land loss (Dietz et al., 2018). A re-nourishment project was initiated in 2012 and completed in 2014 (Coastal Engineering Consultants, 2015), attempting to interrupt the rapid shoreline retreat process and sustain barrier beaches along the Caminada-Moreau headland (Jafari et al., 2018).

The coastal region in southern Louisiana is especially vulnerable to global climate change (Dietz et al., 2018; Johnson et al., 2020), resulting from the Holocene sea-level rise (Kjerfve, 1994). Traditional models have indicated a sea-level 3 to 4 m below present at 6000 years BP, followed by a rise to 1.5 m below present at 5000 BP (Saucier, 1994).

2.2. Physiography

The climate in the study area is humid subtropical, with mean monthly temperatures between 6 °C and 30 °C. The mean precipitation is about 1600 mm/year, with the wetter season from June to September and the drier season from September to June (National Climatic Data Center, 2018). During the last two centuries, the Louisiana coast has been subjected to climatic anomalies (Mock et al., 2007; Perry and Mendelssohn, 2009). The Louisiana coast is frequently affected by severe weather phenomena, including hurricanes, heavy rainfall, flooding, drought, heatwaves, and freezing events (Vega, 2012). Beach fronts and dunes along the Caminada coast support salinity tolerant vegetation, especially graminoid such as cordgrass (*Spartina alterniflora*), sea oats (*Uniola paniculata*), and bitter panicum (*Panicum amarum* var. *amarum* '*Fourchon*'). Cordgrass is found on active overwash deposits (Brantley et al., 2014). Trees and shrubs are mainly represented by wax myrtle (*Myrica cerifera*), iva (*Iva imbricate*), vine (*Lycium barbarum*), eastern baccharis (*Baccharis halimifolia*), and black mangroves (*Avicennia germinans* L.) (Henry and Twilley, 2013). After the restoration project (Coastal Engineering Consultants Inc., 2015), the Caminda coastline has been used for vegetative plantations, including various native dune grass species. Data about the modern American mangrove distribution were obtained at http://data.unep-wcmc.org/datasets/4.

3. Materials and methods

3.1. Remote sensing

The spatial analysis was developed with high-resolution images obtained by the drone Phantom 4 Advanced DJI. This drone had a FC 6310 digital 4K/20MP (RGB), which provided images of high spatial resolution (2.6 cm) of the study area. The drone images were processed using the Agisoft Metashape Professional version 1.6.2 software. The vegetation was visually classified by photointerpretation using various tools in the Global Mapper Software 19. Details about the image processing may be obtained in Cohen et al. (2020a, 2020b).

3.2. Sampling and facies description

Two sediment cores (BC81 - 2,75 m, 29° 6″ 53,10″ N/90° 10′ 33,38″W and BC82 - 4 m, 29° 6″ 48,88′ N/90° 10′ 40,83″ W) were acquired via an aluminum push corer at the southern margin of the BC lagoon (Fig. 1b and c). The cores were measured and photographed in the field and kept in a cold room (4 °C) at Louisiana State University. Grain size analysis (5 cm intervals) was determined by laser diffraction in the Laboratory of Chemical Oceanography of the Federal University of Pará UFPA (Brazil).

Sedimentary features, such as color, texture, lithology, and structure, were used to characterize the facies (Harper, 1984; Walker, 1992). The code of sedimentary facies was based on Miall (1978). The facies, pollen, isotopes, and elemental analyses were grouped into facies associations to determine a sedimentary environment (Reading, 1996). Cluster analysis of pollen grains supported the grouping of the facies associations.

3.3. LOI and XRF data

Loss-on-ignition (LOI) analysis was performed at 1 cm intervals. It involved heating sediment samples at 105°, 550°, and 1000 °C to determine the contents of water, organic matter, and carbonates, respectively. XRF analysis was performed by scanning the core at 2 cm intervals using a handheld Innov-X Delta XRF. Only the major chemical elements in coastal sediments (ppm) representative of marine (e.g. Br, Ca, Cl, and Sr) and terrestrial (e.g. Fe, Ti, and Mn) origins were selected for this analysis (Yao et al., 2015).

3.4. Palynological analysis

The cores were sub-sampled at intervals of 5 cm, whereby 1 cm^3 of sediment was removed for pollen analysis. Before the sediment processing, one tablet of exotic *Lycopodium* spores was inserted into each sample to calculate the pollen concentration (grains/cm^3) and pollen accumulation rates (grains/cm^2/year). Sediment samples were treated following traditional pollen analytical procedures, using hydrochloric acid, hydrofluoric acid, and acetic anhydride/sulfuric acid (Faegri and Iversen, 1989). The product of this treatment was fixed on slides in a glycerin gelatin medium. Pollen and spore morphology books were used as references (McAndrews et al., 1973; Willard et al., 2004), as well as the collections of the LSU Global Paleoecology Lab. A minimum of 300 pollen grains were counted for each sample. The total pollen sum did not include fern spores, algae, and foraminifers. Pollen diagrams are presented as percentages of the total pollen sum. The taxa were categorized into: herbs, trees and shrubs, and aquatics. Cluster analysis and pollen diagram plotting were processed by the software TILIA (Version 1.7.16) (Grimm, 1990).

3.5. Isotopic analysis and radiocarbon dating

The isotopic composition ($\delta^{13}C$) of modern organic matter was analyzed from 134 samples (6–50 mg) taken at 5 cm intervals along the two cores. The stable carbon isotopes were determined at the Stable Isotopes Laboratory of the Center for Nuclear Energy in Agriculture (CENA/USP), using an ANCA SL2020 mass spectrometer (see further details in Pessenda et al. (2004)). Five sediment samples (~2 g each) were used for radiocarbon dating. The samples were physically cleaned using a microscope to prevent natural contamination at ^{14}C Laboratory of CENA (Pessenda et al., 2004). The organic matter was chemically processed by treating with 2% HCl at 60 °C over 4 h, washed with distilled water, and dried (50 °C) to eliminate young organic fractions (fulvic and/or humic acids) and carbonates (Pessenda et al., 2010, 2012). The sediment organic matter was analyzed by Accelerator Mass Spectrometry (AMS) at the ^{14}C Laboratory of CENA/USP, LACUFF (Fluminense Federal University, Brazil), and Center for Applied Isotope Studies (UGAMS) of the University of Georgia. Radiocarbon ages are reported in years before

Table 1
Samples of sedimentary organic matter selected for radiocarbon dating and results with code site, laboratory number, depth (m), ^{14}C ages (yr BP, 1σ), calibrated ages (cal. yr BP, 2σ deviation), sedimentation rate and median of calibrated ages (cal. yr BP).

Sediment core	Code site and laboratory number	Depth (m)	Ages (^{14}C yr BP, 1σ)	Ages (cal. yr BP, 2σ deviation)	Sedimentation rate (mm/yr)	Median of calibrated ages (cal. yr BP)
BC81	UGAMS-34381	170	2150 ± 20	2096–2160	0.76	2128
BC82	UGAMS-34379	170	1580 ± 20	1412–1528	1.1	1470
BC82	LAC 190456	300	5766 ± 48	6406–6645	0.26	6525
BC82	LAC 190457	350	5621 ± 48	6286–6454-		6370
BC82	UGAMS-34380	400	7330 ± 30	8035–8191	0.6	8113

1950 CE (yr BP). The radiocarbon ages were normalized to $\delta^{13}C$ of −25‰VPDB, and are presented in cal yr BP, with a precision of 2σ (Reimer et al., 2013).

4. Results

4.1. Radiocarbon ages and sedimentation rates

Radiocarbon ages and sedimentation rates are provided in Table 1. The ages recorded ranged from 8113 to 1470 cal yr BP (Figs. 2 and 3). Partial age inversions were observed between 350 (6286–6454 cal yr BP) and 300 cm (6406–6645 cal yr BP) (Fig. 3). It can be attributed to high sedimentation rates and/or reworking of organic remains by storms or bioturbation by benthic organisms (Pessenda et al., 2012). The sedimentation rates (0.2 to 1 mm/yr) were within the range recorded in other cores sampled from tidal flats in the Gulf of Mexico (Naquin et al., 2014; Yao et al., 2015). The sedimentation rates in the muddy segment (400–170 cm) of core BC82 were lower (0.6 and 0.26 mm/y) than in the sandy intervals (170–0 cm) of this core (1.11 mm/yr) and core BC81 (0.77 mm/yr) (Figs. 2 and 3).

4.2. Facies description

Three facies associations were recognized in the studied cores (Figs. 4, 5, and Table 2). Facies association A consisted of massive sand (facies Sm) and massive mud (facies Mm), related to a lacustrine environment. Facies association B consisted of lenticular and flaser heterolithic bedded deposits of facies Hl and Hf, respectively, related to a lagoonal environment. Facies association C, which included massive sand (Sm), and flaser heterolithic deposits (Hf), was attributed to washovers. These environments were interpreted based on the integration of sedimentary features with pollen, isotopic, C/N, LOI, and XRF data, as described in the following.

4.2.1. Facies association A (lacustrine)

This facies association was represented by the 400–310 cm interval of core BC82, accumulated between ~8100 and ~6500 cal yr BP. It was characterized by massive mud (Mm) and lenticular heterolithic bedded deposits (Hl; 40–80% silt, 20–60% clay), ranging in color from dark brown (2.5/110Y) to dark gray (3/1 10Y). This facies association contained ~4% of carbonate and ~7% of organic matter. Two ecological groups characterized by herbaceous (25–65%) and tree and shrub pollen (30–55%) were present. The herbaceous taxa were predominantly composed of Amaranthaceae (0–20%), Asteraceae (0–18%), Poaceae (0–12%), *Amaranthus* (0–5%), and *Artemisia* (0–4%). Arboreal taxa were mainly represented by *Pinus* (0–35%), Fagaceae (0–3%), *Betula* (0–1%), and *Quercus* (0–1%). Fern pollen mainly consisted of Polypodiaceae (Fig. 3). XRF analysis indicated the highest concentration of Fe (14 k–20 k ppm), K (8 k–13 k ppm), Ti (1.5 k–2 k ppm), and Mn (370–800 ppm), while the values for Cl (3.5 k–12 k ppm), Ca (5.3 k–8.6 k ppm), Br (184–248 ppm), and Sr (63–98 ppm) were the lowest.

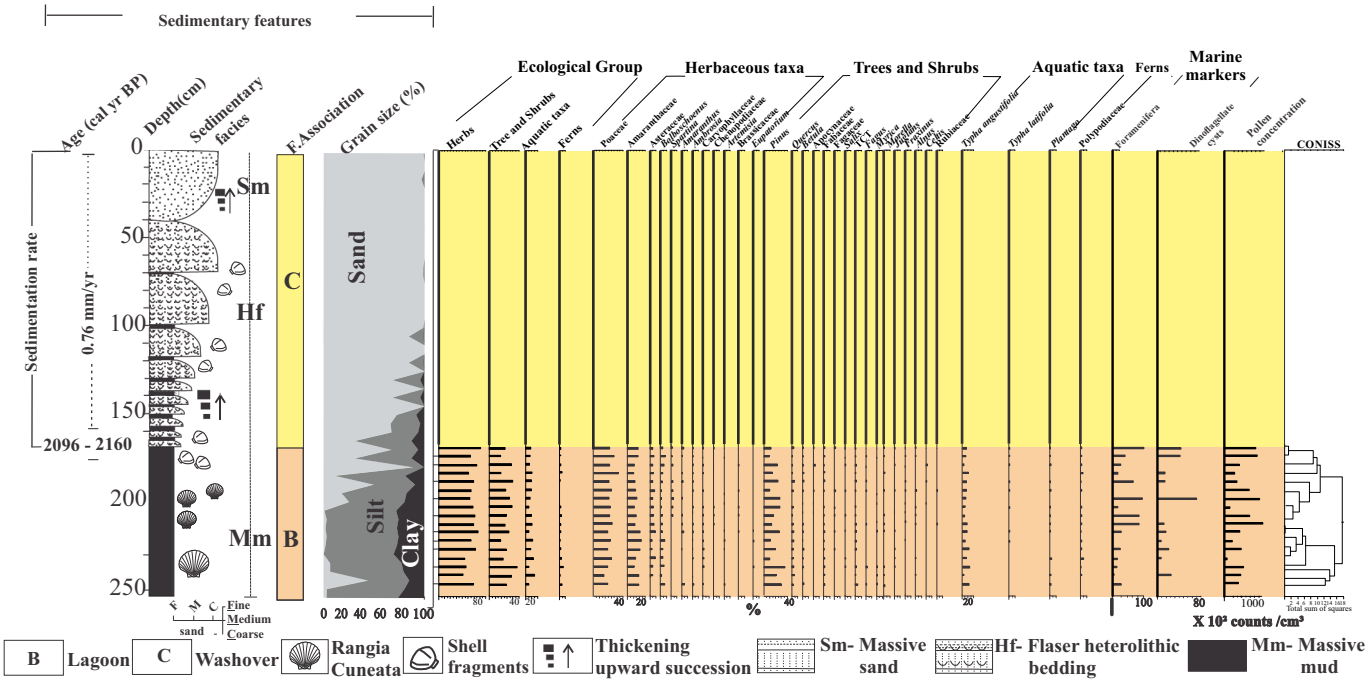

Fig. 2. Stratigraphy of core BC81 exhibiting sedimentary characteristics, facies associations, and pollen data with percentages of the ecological groups. Pollen diagrams are presented as percentages of the total pollen sum.

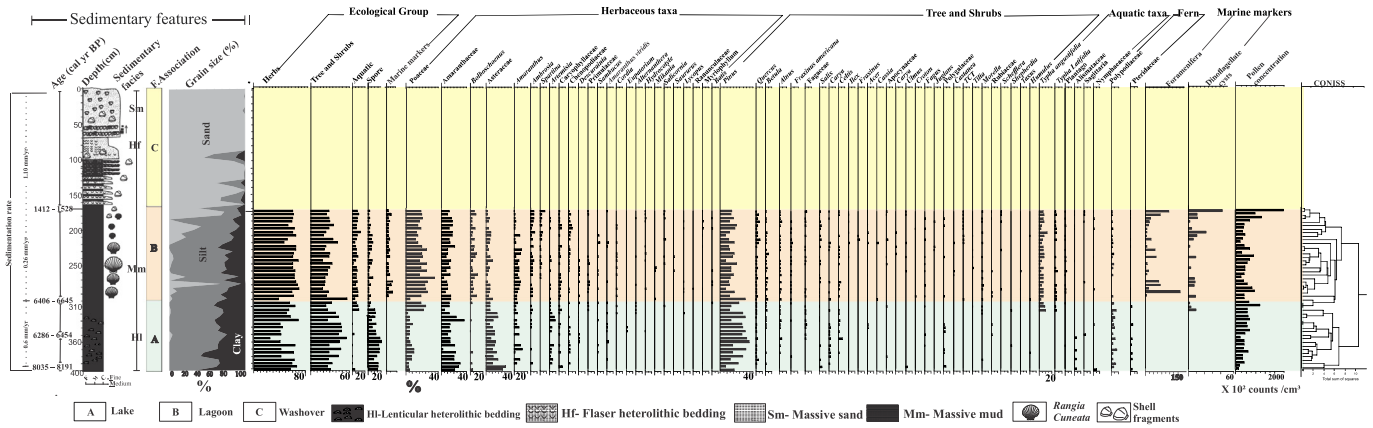

Fig. 3. Stratigraphy of core BC82 exhibiting sedimentary characteristics, facies associations, and pollen data with percentages of the ecological groups. Pollen diagrams are presented as percentages of the total pollen sum.

$\delta^{13}C$ values oscillated between −24.4‰ and −22.02‰ ($\bar{x} = -24‰$), while the C/N ratio alternated between 12 and 52 ($\bar{x} = 25$) (Fig. 5).

4.2.2. Facies association B (lagoonal)

This facies association was evidenced in cores BC81 (270–170 cm) (Figs. 2 and 4), and BC82 (300–170 cm) (Figs. 3 and 5). The sediments were accumulated between ~6525 and ~1470 cal yr BP in core BC82 and up to ~2128 cal yr BP in core BC81. They consisted of dark gray (4/1 10Y) massive mud (Mm) and lenticular heterolithic bedded deposits (Hl; 0–80% sand, 15–80% silt, 5–60% clay). This facies association contained ~4% of carbonate and ~7% of organic matter. The bivalve *Rangia cuneata* was present in life position. The palynological analysis permitted the identification of three ecological groups, represented by pollen of herbs (50–70%), trees and shrubs (20–55%) and aquatic plants (2–10%), in addition to marine markers, such as dinoflagellate cysts and foraminifera. Herbs were mainly represented by Poaceae (0–25%), Amaranthaceae (0–14%), Asteraceae (0–6%), *Amaranthus* (0–4%), *Ambrosia* (0–4%), *Bolboschoenus* (5%), Caryophyllaceae (2%), *Spartina* (0–3%) and Chenopodiaceae (0–2%). Arboreal pollen included mainly *Pinus* (0–20%), *Quercus* (0–3%), *Betula* (0–3%), and *Alnus* (0–2%). The group of aquatic plants was predominantly composed of *Typha angustifolia* (0–14%) and *Typha latifolia* (0–3%) (Figs. 2 and 3). *Typha angustifolia* disperses as a reticulate, monoporate monad pollen (22.7 ± 2.6 μm) (Fig. 1a and b, supplementary material), and *Typha latifolia* is reliably represented in the pollen record as perforate-reticulate, tetrads pollen (25.70 ± 1.58) (Finkelstein, 2003; Hamdi et al., 2010; Skvarla and Larson, 1963) (Fig. 1c and d, supplementary material). XRF results revealed an increasing trend in Cl (3 k–20 k ppm) and Br (190–950 ppm) and a decreasing trend in Fe (7 k–17.5 k ppm) and Mn (186–500 ppm) compared to facies association A. Facies association B presented more enriched $\delta^{13}C$ values (~ −22‰) than the facies association A (~−24‰). C/N values decreased upward from ~25 to ~11 within this association (Figs. 4 and 5).

4.2.3. Facies association C (washover)

These deposits were identified in both studied cores in the interval 170–0 cm, formed during the last ~1470 cal yr BP (170–0 cm) and ~2100 cal yr BP in the cores BC82 and BC81, respectively. The cores consisted of dark gray (4/1 10Y) flaser heterolithic bedded deposits (facies Hf; 60–100% sand, 0–40% silt, 0–10% clay); sandy layers were cross laminated. The upper part of facies association A was characterized by massive sand (Sm; 14% coarse, 73% medium, 13% fine); grain size increased gradually upward in this sandy facies. Shell fragments were frequent in this association. The carbonate concentration oscillated between 4 and 20%, while the organic matter decreased upward from 4 to 2%. A wide range of variation was recorded for the concentrations of Ca (2.7 k–130 k ppm), Sr (100–572 ppm), Zn (0–46 ppm), and Zr (44–422 ppm). The concentration of Ti (270–1134 ppm), and Fe (2100–7200 ppm) also varied largely, but with values that were lower than in facies associations A and B. $\delta^{13}C$ and C/N values oscillated between −20 and −27‰ and 3 and 28, respectively. No pollen grain was found in this facies association (Figs. 4 and 5).

5. Discussion

The sampling sites are accumulating washover sediments at present (Fig. 1b and c). These sites were chosen due to their position in the central

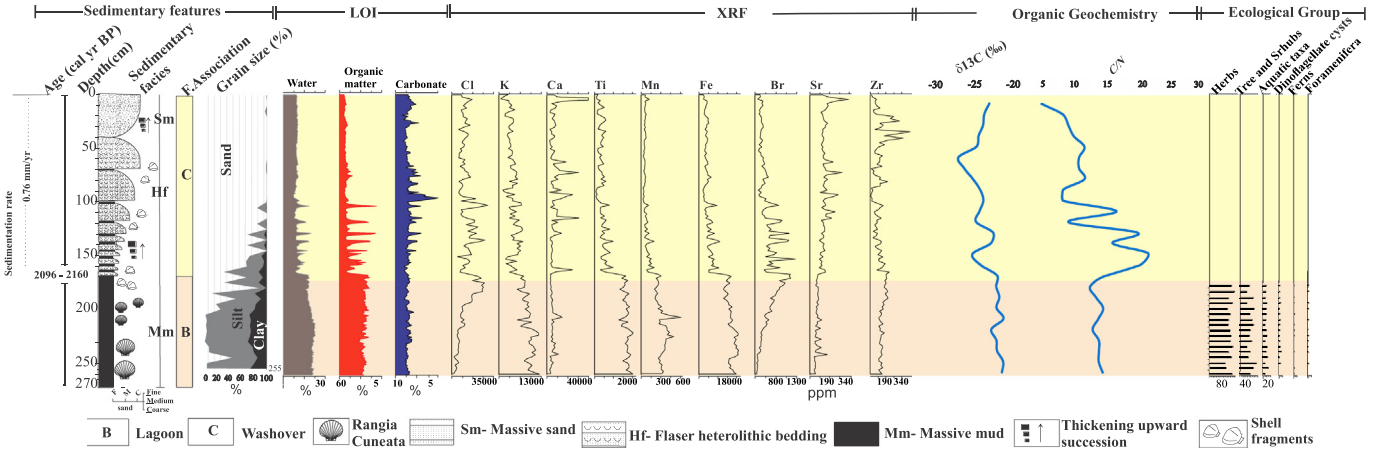

Fig. 4. Summary of core BC81, presenting sedimentary characteristics, pollen ecological groups, and geochemical data.

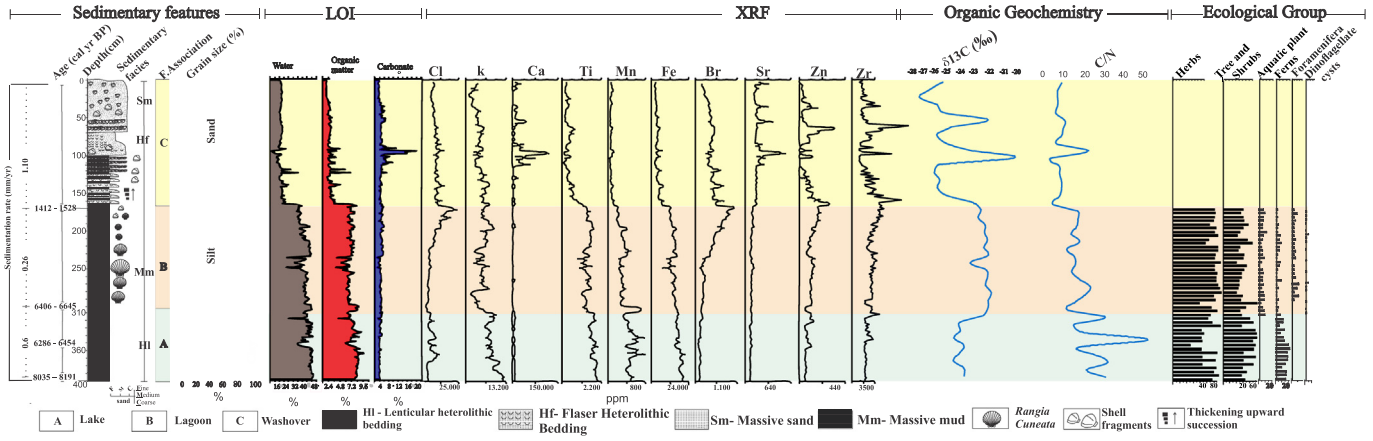

Fig. 5. Summary of core BC82, presenting sedimentary characteristics, pollen ecological groups, and geochemical data.

portion of an old lake (Fig. 7), with the potential to preserve the oldest lacustrine records. Depositional environments with a predominance of sandy sediments are not suitable for preserving pollen grains (Havinga, 1967). However, such environment may have evolved from an environment with low hydrodynamic flow that was favorable for the muddy (silt and clay) sedimentation (Reineck and Singh, 1980; Reading, 1996) and suitable for pollen preservation, as indicated by several pollen studies in tidal flats (Behling et al., 2001, 2004; Cohen et al., 2005a, 2005b, 2012, 2020b; Guimarães et al., 2013; Moraes et al., 2017; Ribeiro et al., 2018), fluvial flood plains (Cohen et al., 2014a, 2014b, 2014c, 2020a; Fontes et al., 2017; Lima et al., 2017; Silva et al., 2018), lagoons (Cohen et al., 2020b, 2016; França et al., 2016), and lakes (Lara and Cohen, 2009; Smith et al., 2011; Buso Junior et al., 2013). For example, oxbow lakes, developed after a channel abandonment, can be filled by muddy sediments and converted into a fluvial terrace or an active channel with sandy deposition (Cohen et al., 2014c; Rossetti et al., 2014). In the case of the study area, evidence based on facies association indicated the development of a lake (~8100 to ~6500 cal yr BP), which subsequently evolved into a lagoon (6500–1470 cal yr BP). Relatively high pollen concentrations (50 k–200 k pollen grains/cm^3, Figs. 2 and 3) in the sediments from this period suggested that the land around the lake and lagoon was well-vegetated. Gradually over the last ~1470 cal yr BP, this coastal lake and lagoon at the coring site has been filled by washover sandy sediment, which was not conducive to retention and preservation of pollen.

5.1. Depositional phases

5.1.1. Early Holocene (~8100 to ~6500 cal yr BP): lacustrine

The prevalence of muddy deposits in facies association A (i.e., basis of core BC82, 400–310 cm) indicates a low energy depositional environment, most likely a freshwater lake. The $\delta^{13}C$ and C/N, ranging from −24.4 to −22.02‰ and 12 to 52 respectively, recorded in these deposits support that C3 terrestrial plants were the source for the sedimentary organic matter (C3 plants $\delta^{13}C$: −32‰ to −21‰ and C/N: >12; Deines, 1980; Meyers, 1994; Tyson, 1995). The concentrations of K, Ti, Fe, and Mn in facies association A were compatible with values recorded in environments with a high input of terrestrial sourced sediment (Cuven et al., 2013; Yao et al., 2018). The presence of arboreal pollen from *Pinus*, *Quercus*, Fagaceae, and *Betula*, as well as herbs (mainly represented by Asteraceae and Amaranthaceae) and wetland ferns (represented by Polypodiaceae), conforms with a freshwater, terrestrial setting. Altogether, these characteristics are taken as evidence of a lacustrine environment for facies association A. The inferred lake developed in the study area during the early Holocene when the sea-level was ~8 m below the modern sea-level (Donoghue, 2011) (Fig. 7).

5.1.2. Mid-late Holocene (~6500 to ~1470 cal yr BP): lagoonal

This phase is recorded by facies association B, which is lithologically similar to the lacustrine deposits characterized by the prevalence of muddy components (facies Mm and Hl) indicating low energy environments. However, the presence of the bivalve *Rangia cuneata* attests to a connection to marine waters, as this species is typical of brackish water environments (Tarver, 1972; Warzocha et al., 2016). This bivalve, native to the Gulf of Mexico (Benson, 2010), has often been used to indicate marine influence during the Holocene (Rodriguez et al., 2004; Wakida-Kusunoki and MacKenzie, 2004). Accordingly, we interpret facies association B to represent a lagoon. The slight enrichment of $\delta^{13}C$ values in facies association B (~−22‰) compared to the lacustrine deposits (−24‰), and the decreasing C/N values from ~25 to ~9, suggest the contribution of marine organic matter ($\delta^{13}C$: −24‰ to −16‰ and

Table 2
Characteristics of the three facies association.

Facies association	Facies description	Ecological group	Geochemical data	Elements predominance (ppm)	Interpretation
A	Lenticular heterolithic bedding (facies Hl)	Herbs, tree/shrubs, and ferns	$\delta^{13}C = -24.4$ to −22‰ C/N = 12–2	Fe: 14 k–20 k K: 8 k–13 k Ti: 1.5 k–2 k Mn: 370–800	Lake
B	Massive mud (facies Mm) with *Rangia cuneata*	Herbs and aquatic plants from brackishwater. Foraminifera/dinoflagellate	$\delta^{13}C = -23$ to −21‰ C/N = 6–22	Cl: 3 k–20 k Br: 190–950 Fe: 7 k–17.5 k Mn: 186–500	Lagoon
C	Flaser heterolithic bedding (Hf), massive sand (Sm) with shell fragments	No pollen/ferns	$\delta^{13}C = -27$ to −20‰ C/N = 5–20	Cl: 6 k–24 k Ca: 2.7 k–130 k Br: 230–1200 Sr: 100–572 Zr: 44–422	Washover

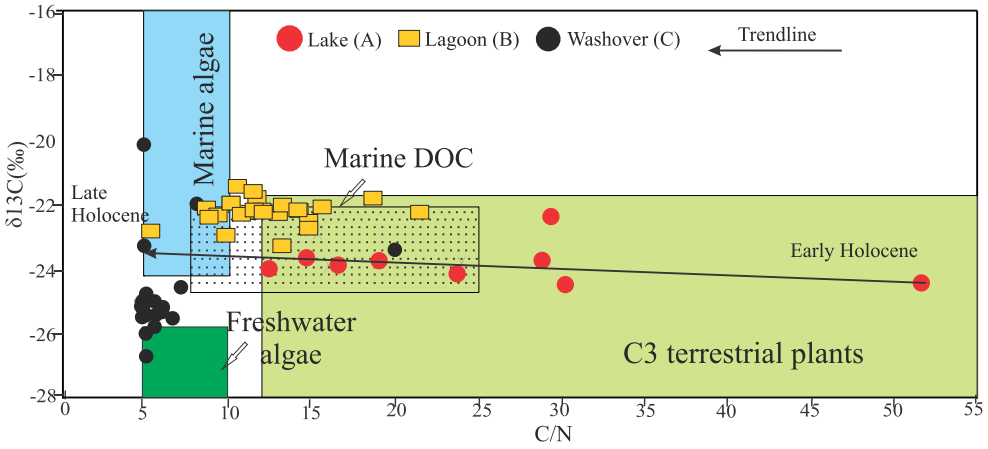

Fig. 6. Binary diagram showing the source of the sedimentary organic matter for each sedimentary facies associations based on the relationship between $\delta^{13}C$ and C/N.

C/N: <10; Deines, 1980; Meyers, 1994; Tyson, 1995) (Fig. 6), as expected in a lagoon. The upward increase of Cl (from 4 k to 13 k ppm) and Br (from 264 to 950 ppm) and decrease of Fe (from 16 k to 11 k ppm) and Mn (from 400 to 200 ppm) are also indications of a coastal environment with marine influence and lower input of terrestrial sediments. The pollen assemblage, marked by the increased abundance of brackishwater herbaceaous (*Bolboschoenus*, *Spartina*) and brackishwater aquatic (*Typha angustifolia* and *Typha latifolia*) plants, is further consistent with the inferred lagoon environment. The aquatic macrophyte cattail (*Typha*) can tolerate environments with high salinity (Hameed et al., 2012; Akhtar et al., 2017) and variation in water level (Ladislas et al., 2012). Paleoecological studies in brackish lagoonal deposits from Mexico also indicated the establishment of *Typha* ~6000cal yr BP (Caballero et al., 2005). In addition, the occurrence of foraminifera and dinoflagellate cysts in this stratigraphic unit is further evidence for a marine-influenced environment, such as a lagoon.

5.1.3. Late Holocene (last ~1470 cal yr BP): shoreline retreat

This phase is recorded by facies association C, whereby the muddy deposits changed abruptly upward into heterolithic mud/sand and massive sand. It represents the modern washover sediments that are deposited inland of a beach by overwash. Overwash is the flow of water and sediment over the beach's crest that does not return to the water body. Coastal overwash is mainly caused by hurricanes and winter storms along the Atlantic and Gulf Coasts of the United States (Liu, 2004; Donnelly et al., 2006). This sedimentary succession may reflect the gradual landward migration of sandy coastal barriers due to marine transgression (Fig. 7). This interpretation is based on the increased marine influence with respect to the lagoon deposits of the previous phase. This is evidenced by the lower input of terrestrially-sourced sediments evidenced by the decreasing trend of Ti (1700 to 400 ppm), Fe (from 12 k to 2 k ppm), and Mn (from 230 to 75 ppm) and strong oscillations of Ca (2 k–129 k ppm), Cl (5.6 k–24 k ppm), Sr (100–572 ppm), Br (230–1200 ppm), Zn (0–46 ppm), and Zr (44–422 ppm). High Zn and Zr values are found in the sand fraction. Then, probably, oscillations of Zn and Zr values indicated phases of rock weathering carried by the action of the currents and tides and deposited as beach sand. Ca, Cl, Br, and Sr are constituents of biogeochemical cycling in marine systems (Yao and Liu, 2017; Joe-Wong et al., 2019). The significant decrease in C/N values, from ~10 to ~6, with respect to the lagoonal phase, and the $\delta^{13}C$ values, between −20‰ and −27‰, are consistent with this interpretation (marine algae, $\delta^{13}C$: −24‰ to −16‰ and C/N: <10) (Deines, 1980; Meyers, 1994; Tyson, 1995) (Fig. 6). Local oscillations of these values that were synchronized with Ca, Sr, Zn, and Zr peak concentrations are probably a result of storm events, since this coastline is notably affected by intense hurricanes and tropical storms (Dietz et al., 2018; Johnson et al., 2020).

5.2. Absence of mangrove pollen along the cores

The analyzed cores did not contain mangrove pollen grains, despite the dense occupation of *Avicennia* trees around the lagoon nowadays. Noteworthy is that lakes, lagoons, tidal flats, and fluvial floodplains present suitable hydrodynamic conditions for muddy sedimentation with pollen derived from plants that lived at the times the sediments were deposited. Under this situation, lagoonal and lacustrine sediments preserve pollen grains transported by wind and from the flora surrounding the lake or lagoon. The spatial representation of lagoonal or lacustrine pollen records changes according to the wind intensities and the watershed area influencing the lake or lagoon (Cohen et al., 2008, 2014c). In addition, the pollen percentage of each vegetation unit is distance-weighted, where the closer to the source, the greater the pollen signal from that plant (Davis, 2000; Xu et al., 2012). Thus, pollen accumulated in lagoon or lake sediments presents a wider spatial representation of the regional flora than tidal flats sediments. Pollen rain in tidal flats, mainly occupied by dense mangrove forests, should indicate local vegetation, while open canopy tends to present a higher proportion of long distance transport pollen rain (Weng et al., 2004; Gosling et al., 2009).

Considering the pollen grains can be transported by wind and currents mainly in open areas (Brush and Brush, 1972; Solomon et al., 1982; Weng et al., 2004), it is common to record <1% pollen grains that do not represent the local vegetation during the sediment accumulation. For instance, a core taken from a marsh in southwestern Louisiana revealed one or two *Avicennia* pollen grains in the 0, 210, and 280 cm depth, probably transported by currents or hurricanes (Yao et al., 2020). By contrast, cores taken from tidal flats occupied by mixed mangroves with *Rhizophora*, *Laguncularia*, and *Avicennia* in Florida contained pollen percentages of 30–60% of *Rhizophora*, 5–20% of *Avicennia*, and 5–15% of *Laguncularia* (Yao et al., 2015; Yao and Liu, 2017). The lagoon and tidal flat sediments covered by *Avicennia* trees in Bay Champagne, the study area, accumulate between 6 and 9% of *Avicennia* pollen (Ryu, 2020). In Amazonian mangroves, pollen traps installed on tidal flats occupied only by *Avicennia* trees present ~15% (~540 grains/cm^2/yr) of *Avicennia* pollen (Behling et al., 2001). Accumulation rates of *Avicennia* pollen are also relatively elevated in a mangrove with *Rhizophora* and *Avicennia* trees (average 450 grains/cm^2/yr). Even in mangroves dominated by *Rhizophora*, pollen grains of *Avicennia* may be found (average 120 grains/cm^2/yr) (Behling et al., 2001). In addition, *Avicennia* pollen grains have been found in thousands of stratigraphic pollen spectra obtained from cores sampled from the American coasts with *Avicennia* trees (e.g. Cohen et al., 2005a, b, 2009, 2012, 2014a, b, c, 2015, 2016; Vedel et al., 2006; Peros et al., 2007; Guimarães et al., 2011, 2013; Smith et al., 2011, 2012; França et al., 2014, 2016, 2019; Yao et al.,

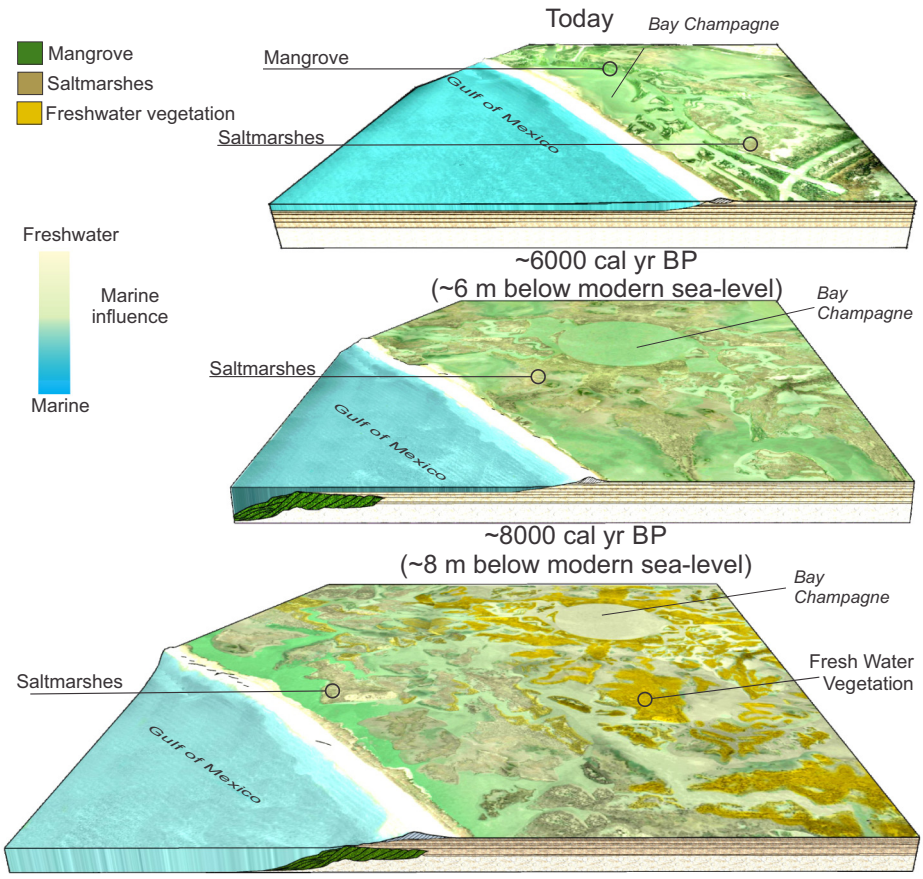

Fig. 7. Model of the geomorphology and vegetation development under the Holocene relative sea-level rise.

2015; Yao and Liu, 2017; Moraes et al., 2017; Ribeiro et al., 2018; Cordero-Oviedo et al., 2019; Jones et al., 2019).

These data suggest that sediments accumulated in tidal flats or lagoons with *Avicennia* or near *Avicennia* trees tend to have a significant *Avicennia* pollen representation. Therefore, the absence of *Avicennia* pollen grains in the sedimentary sequences formed during the lake (8100–6500 cal yr BP) and lagoon (6500–1470 cal yr BP) phases in our cores (Figs. 2 and 3) suggests that mangroves with *Avicennia* trees were absent at or near our study site during the Holocene.

The absence of mangroves in the modern northern limit of American mangroves between ~8100 and ~1470 cal yr BP is an important finding that contributes significantly to the discussions about the main forces driving the mangrove establishment on the American continent during the Holocene, as well as its poleward expansion in the Anthropocene (since the mid-twentieth century (Zalasiewicz et al., 2018)). Nevertheless, it is necessary to assess the effects of sea-level rise on the studied coastal vegetation and morphology, since the salinity gradients along the zones under marine or estuarine influence need to be conducive to mangrove development (Lara and Cohen, 2006).

5.3. American mangrove establishment controlled by sea-level

Mangroves colonized the distal portion of the continental shelf during the Last Glacial Maximum (LGM) (~27 and ~20 k cal yr BP) due to the worldwide lowering of the eustatic sea-level (Murray-Wallace, 2007; Cohen et al., 2014a, 2014b, 2014c). The continental shelf emerged almost completely, positioning the coastline at some sites ~100 km of its current location (Nittrouer et al., 1996; Clark et al., 2009; Harris et al., 2013). After the LGM low sea-level, melting ice sheets caused transgression between 16 and 4 ka in many areas of southern North America (Gischler, 2015) and, probably, a landward mangrove migration along the continental shelf (Cohen et al., 2012, 2014b). A rapid relative sea-level rise was recorded on the eastern coast of South America during the early-middle Holocene. The sea-level in southeastern and northeastern Brazilian coast was between 5 and 1 m above the modern sea-level, at approximately 5500 cal yr BP, with a gradual fall during the middle to late Holocene (Angulo et al., 2006, 2016; Caldas et al., 2006; Lorente et al., 2013; Cohen et al., 2020a). Sea-levels comparable to the modern one were already reached between 6000 and 5000 cal yrs BP in the northern Brazilian coast (Cohen et al., 2005b, 2012). Several works have attributed the mangrove establishment in the middle Holocene along the tropical coasts to the lower rates of sea-level rise or a stable sea-level in the middle Holocene (Woodroffe et al., 1985, 2015; Toscano and Macintyre, 2003; Khan et al., 2017; Ribeiro et al., 2018; Cohen et al., 2020a) (Fig. 8). Then, mangroves were established in the tropical Brazilian littoral at ~7000 cal yr BP: Espírito Santo (19° S), Bahia (17° S), Rio Grande do Norte (5° S), Pará (1° S), and Amapá (2° N) (Cohen et al., 2012, 2014a, 2014b, 2020a; Pessenda et al., 2012; França et al., 2013, 2015; Fontes et al., 2017; Ribeiro et al., 2018).

Similarly, transgressive events were also recorded in the northern Gulf of Mexico (Anderson and Fillon, 2004), with a high sea-level rise rate of 7.4 ± 0.7 m/ka in the early Holocene, and a reduced rate of 2.3 mm/yr in the middle to late Holocene (Wanless et al., 1994; Khan et al., 2017). The relative stability of modern coastal systems along the Gulf of Mexico is primarily due to the stabilization of sea-level approximately 6000 years ago (Donoghue, 2011). Blum et al. (2002) proposed that the middle Holocene sea-level along the Texas Gulf coast was at −9 m at ca. 7.8 ka, then rose rapidly to +2 m by ca. 6.8 ka. However, according to Khan et al. (2017), the relative sea-level did not exceed the present height during the Holocene, and around ~6.5 ka, sea-level was at 6.2 m below the modern sea-level (Willard and Bernhardt, 2011). The sea-

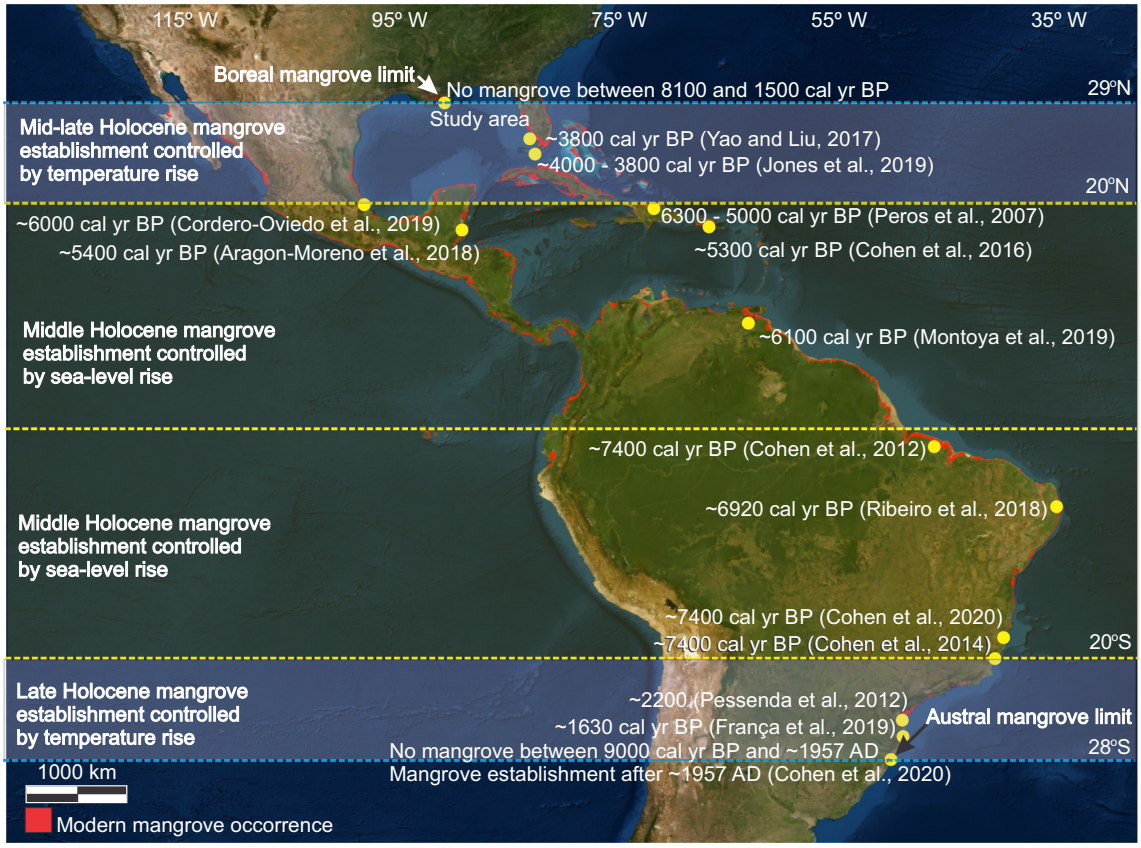

Fig. 8. American mangrove distribution in the tropical and subtropical zones and time of the mangrove establishment during the Holocene. The modern American mangrove distribution was obtained at http://data.unep-wcmc.org/datasets/4.

level, which was near the modern level during the middle Holocene, allowed mangrove establishment in the Caribbean and Gulf of Mexico coast, a tropical zone, at ~6100, ~5400, ~5300, and ~5500 cal yr BP, in Venezuela (9° N), Puerto Rico (18° N), Yucatan Peninsula-Mexico (18°–21° N) and Cuba (22° N), respectively (Peros et al., 2007; Cohen et al., 2016; Aragón-Moreno et al., 2018; Montoya et al., 2019). In addition, mangroves were recorded in the western Gulf of Mexico coast (20° N) at ~6000 cal yr BP (Cordero-Oviedo et al., 2019).

In the study area (29° N), marine transgression caused the development of lagoons and saltmarshes with a strong contribution of marine organic matter after ~6500 cal yr BP (Figs. 4, 5, 6, and 7). This sedimentary environment associated with vegetation and sedimentary organic matter suggests favorable physical-chemical conditions for mangrove establishment. Therefore, of the sea-level dependent factors, mangroves could have been established in the study area since ~6500 cal yr BP. However, contrasting with the tropical coasts, there was no evidence of mangrove presence around the Bay Champagne lagoon, the current northern mangrove limit, between 6500 and 1470 cal yr BP. A similar situation occurred at the southern limit of American mangroves at Laguna, southern Brazilian coast (28° 29′ S), where pollen studies also indicate the absence of mangroves during the Holocene. Mangroves were established at their current southern limit of South America only in the Anthropocene (Cohen et al., 2020b). Probably, despite the physical-chemical conditions suitable for mangrove establishment promoted by the sea-level rise, the temperature may not yet have been high enough to allow the growth of mangroves at their current northern and southern limits of American mangroves during the middle-late Holocene. In addition, biogeographic studies indicated that modern global distribution of mangroves is mainly controlled by temperature, hence being limited to tropical and subtropical regions (Lugo and Patterson-zucca, 1977; Sherrod and McMillan, 1985; Duke et al., 1998; Stevens et al., 2006; Stuart et al., 2007).

5.4. Mangrove establishment controlled by climate

Considering that mangroves are susceptible to changes in sea-level and climate in a millennial timescale (Chapman, 1975; Duke, 1992; Blasco, 1996; Fromard et al., 2004; Alongi, 2008), and to local factors in a secular/decadal time scale (Moraes et al., 2017; Ribeiro et al., 2018) the (1) presence or (2) absence of mangroves along their current northern and southern limits during the Holocene is essential to identify the reasons for the mangrove expansion to more temperate zones during the recent decades. Regarding the hypothesis of the (1) continuous presence of mangroves in the current northern (29° N) and southern (28° S) boundaries of the American continent (North and South America) during the middle-late Holocene, it would indicate relative stability of relative sea-level and climate during that period. In this case, studies that show the poleward mangrove expansion during the most recent decades (e.g. Cavanaugh et al., 2014; Saintilan et al., 2014; Osland and Feher, 2020) could be incorrectly attributing such mangrove dynamics to allogeneic processes, for instance, global warming. Alternatively, it may be caused by autogenic mechanisms, for instance, related to the action of tides, storms, dynamics of beach-barrier, delta switching, and lateral migration of meandering fluvial channels, then creating and destroying mangrove substrates in a cyclical process with expansion and contraction phases of mangrove areas in a decadal time scale (Moraes et al., 2017). In this context, such mangrove expansion would be related to processes operated locally and intrinsic to the depositional system (Beebower, 1964; Cecil, 2013).

By contrast, the (2) absence of mangroves in their current northern and southern limits in the Holocene indicates an allogeneic process driving the mangrove expansion from tropical into temperate latitudes in a millennial time scale. In general, the geological record suggests equatorward contraction of mangroves during the LGM (Woodroffe and Grindrod, 1991; Cannon et al., 2009), when these forests occurred

only in refuge areas more protected from the impact of cold air temperature (Cannon et al., 2009). In contrast, a poleward mangrove expansion occurred after the LGM (Sandoval-Castro et al., 2012; Kennedy et al., 2016). During the early and middle Holocene, this trend may have been favored in tropical to subtropical areas by increasing the global mean surface temperature (O'ishi and Abe-Ouchi, 2011; Fig. 8).

There is a consensus about global warming between the LGM and early Holocene (Kaufman et al., 2020). However, less well understood is the climate between the mid and late Holocene (Sundqvist et al., 2014). The Antarctic Peninsula underwent an early-Holocene warm phase and stable temperatures between 9200 and 2500 years ago (Mulvaney et al., 2012). Studies over land north of 40°N have indicated warming during the middle Holocene (O'ishi and Abe-Ouchi, 2011). Other proxy records indicated global cooling during the late Holocene (Marcott et al., 2013). However, with no direct net contribution from the orbitally-driven insolation, the global annual mean radiative forcing in the Holocene should be dominated by the retreating ice sheets and rising atmospheric greenhouse gases, with both favoring a globally averaged warming (Liu et al., 2014). Climate models simulate a robust global annual mean warming along the Holocene, mainly in response to rising CO_2 and the retreat of ice sheets (Liu et al., 2014). Other climate models suggest no change or warming during the mid-late Holocene (Braconnot et al., 2007; Timm and Timmermann, 2007; Lohmann et al., 2013). The increase of CO_2 and CH_4 concentrations after 7000 and 5000 years ago contributed to the late Holocene warmth, prolonging the natural interglacial warmth initiated by orbital variations. These mid-late Holocene greenhouse gas increases may be natural or anthropogenic in origin (Ruddiman, 2003; Broecker and Stocker, 2006; Kaplan et al., 2011; Ruddiman et al., 2016). A stable isotope record from ice wedges from the Arctic indicated a long-term winter warming trend during the mid-late Holocene (Meyer et al., 2015). $\delta^{18}O$ of planktonic foraminifera from the western tropical South Atlantic Ocean on the northeast Brazilian margin showed a progressive warming trend of slightly >1 °C during the transition from the mid- to late-Holocene (Santos et al., 2013). A record of Holocene sea-surface temperatures and sea-ice presence from the Polar Front of the East Atlantic Southern Ocean showed late Holocene warming and no abrupt Neoglacial cooling (Nielsen et al., 2004). Jomelli et al. (2011) proposed Holocene warming for the eastern tropical Pacific with increased atmospheric temperature and retreat of glaciers in the southern tropics in response to enhanced austral summer insolation. This Holocene climate trend indicated by the climate models and proxy records is consistent with the hypothesis that climate warming permitted mangroves to expand from the tropics to subtropics during the mid-late Holocene (Fig. 8).

Although the coastal stabilization or low rates of sea-level change around the middle Holocene may have played a role in the establishment of northern and southern American mangroves in areas located between the latitude of 20°N and 20°S, the subtropical mangroves were established only in the mid-late Holocene in both hemispheres, probably as a result of global warming that caused a poleward mangrove expansion from the latitude of 20° to 29°. The mangroves in the subtropical Brazilian coast were established between ~2200 cal yr BP (São Paulo, 25° S) and ~1630 cal yr BP (Santa Catarina-Brazil, 26° S) (Pessenda et al., 2012; França et al., 2019), and the subtropical mangroves in North America appeared after ~4000 cal yr BP in the Everglades-Florida (25° N) (Willard and Bernhardt, 2011; Yao et al., 2015; Yao and Liu, 2017; Jones et al., 2019) (Fig. 8). Regional-scale droughts may have some influence in delaying the mangrove establishment in the subtropical mangroves of the Everglades (Willard and Bernhardt, 2011), but global warming in the mid-late Holocene must be considered as the main force favoring the mangrove expansion from tropical to subtropical areas in both hemispheres.

Our study shows the absence of mangroves between ~8100 and ~1500 cal yr BP in Port Fourchon (29° 09′ N), USA. The first evidence of black mangroves in Louisiana was dated at approximately 1900 CE (Lloyd and Tracy, 1901). These authors described early mangrove stands short in stature (<0.6 m) growing on offshore islands, mainly in Breton Sound. In addition, a historical video of the U.S. Library of Congress (http://www.loc.gov/item/mp76000363) also exhibited black mangroves at the Breton National Wildlife Refuge in Louisiana in 1915. Similarly, in the southern limit of the American mangroves at Laguna, Brazil (28° 29′ S), even though physicochemical and hydrodynamic conditions were favorable for the establishment and expansion of mangroves since the middle Holocene, mangrove establishment occurred only between ~1957 and ~1986 CE (Cohen et al., 2020b). It is noteworthy that a subtropical Brazilian mangrove stand (26° S), established since ~1630 cal yr BP, contained *Rhizophora* trees only during the last decades (França et al., 2019). *Rhizophora* is less tolerant to low temperatures than *Laguncularia* and *Avicennia* (Duke et al., 1998; Quisthoudt et al., 2012). The presence of mangroves in Louisiana, even incipient and restricted to some islands since the beginning of the 20th century, suggests that this ecosystem was established only after appropriate climatic conditions were present since that time.

We propose that the establishment of *Avicennia* trees in the study area was related to the natural warming trend after the Little Ice Age (LIA). This cold climatic episode was attributed to solar activity fluctuations during the last six or seven centuries (Lean and Rind, 1999), ending between 1850 and 1890 CE (Bradley and Jones, 1992). Ongoing remote sensing work (unpublished) by Cohen and co-workers indicates a significant increase in the area and stature of Louisiana mangroves in recent decades, especially in the 21st century. Therefore, while our data suggest that a poleward mangrove migration occurred due to natural global warming during the late Holocene, the industrial-era warming must have intensified the mangrove expansion during the last few decades, when temperature increased at a higher rate in the boreal and temperate regions than in the tropics (Solomon et al., 2007).

6. Conclusions

Our integrated multi-proxy investigation based on sedimentology, ^{14}C radiocarbon dating, pollen analysis, as well as X-ray fluorescence, isotope ($\delta^{13}C$), and C\N data indicate a marine transgression at Bay Champagne, Louisiana-USA during the Holocene. This natural process changed the environment from a freshwater lake (~8100 to ~6500 cal yr BP) to a brackish water lagoon (~6500 to ~1500 cal yr BP). During the last ~1500 cal yr BP, washover sand was deposited into the lagoon due to the relative sea-level rise and hurricanes. Physicochemical and hydrodynamic conditions suitable for mangrove development occurred in the study site over the last ~6500 cal yr BP. However, mangrove pollen were not recorded in sediments between ~8100 and ~1500 cal yr BP, suggesting that mangroves were absent during the entire period. A comparative analysis of these multi-proxy data and historical records of mangrove establishment phases in the Gulf of Mexico, Caribbean, and eastern South America indicated that mangroves expanded gradually from the tropical to subtropical South and North American coasts during the mid and late Holocene. The modern boreal (29° 09′ N) and austral (28° 29′ S) mangrove limits were established in the early and mid-20th century, respectively. This mangrove dynamics on a continental scale suggests that poleward mangrove migration was caused by natural Holocene global warming. The industrial-era warming must have intensified the mangrove expansion. However, the Anthropocene global warming was not a direct forcing that initiated the mangrove migration into temperate zones.

Supplementary data to this article can be found online at https://doi.org/10.1016/j.geomorph.2021.107648.

Declaration of competing interest

The authors declare that they have no known competing financial interests or personal relationships that could have appeared to influence the work reported in this paper.

Acknowledgments

The authors thank the Graduate Program in Geology and Geochemistry of the Federal University of Pará. We also acknowledge the logistic support provided by the College of the Coastal and Environment of the Louisiana State University. This study was financed by the Brazilian Council for Technology and Science-CNPq (Project # 307497/2018-6), FAPESP 2017/03304-1, the U.S. National Science Foundation (NSF Project # 1759715), the Ministry of Science and Technology of the People's Republic of China (Project # 2017YFE0107400), and NOAA through the Louisiana Sea Grant (Project #2013-39).

References

Akhtar, N., Hameed, M., Nawaz, F., Ahmad, K.S., Hamid, A., Segovia-Salcedo, C., Shahnaz, M.M., 2017. Leaf anatomical and biochemical adaptations in *Typha domingensis* Pers. ecotypes for salinity tolerance. Bot. Sci. 95, 807–821. https://doi.org/10.17129/botsci.886.

Alongi, Daniel M., 2008. Mangrove forests: resilience, protection from tsunamis, and responses to global climate change. Estuar. Coast. Shelf Sci. 76, 1–13. https://doi.org/10.1016/j.ecss.2007.08.024.

Alongi, D.M., 2015. The Impact of climate change on mangrove forests. Curr. Clim. Chang. Rep. 1, 30–39. https://doi.org/10.1007/s40641-015-0002-x.

Amaral, P.G.C., Ledru, M.-P., Branco, F.R., Giannini, P.C.F., 2006. Late Holocene development of a mangrove ecosystem in southeastern Brazil (Itanhaém, state of São Paulo). Palaeogeogr. Palaeoclimatol. Palaeoecol. 241, 608–620. https://doi.org/10.1016/j.palaeo.2006.04.010.

Anderson, J.B., Fillon, R.H., 2004. Late Quaternary stratigraphic evolution of the northern Gulf of Mexico margin. SEPM (Soc. Sedimen. Geol.) 79, 311.

Angulo, R., Lessa, G., Souza, M., 2006. A critical review of mid- to late-Holocene sea-level fluctuations on the eastern Brazilian coastline. Quat. Sci. Rev. 25, 486–506. https://doi.org/10.1016/j.quascirev.2005.03.008.

Angulo, R.J., Giannini, P.C.F., Souza, M.C. De, Lessa, G.C., Angulo, R.J., Giannini, P.C.F., Souza, M.C. De, Lessa, G.C., 2016. Holocene paleo-sea level changes along the coast of Rio de Janeiro, southern Brazil: comment on Castro et al. (2014). An. Acad. Bras. Cienc. 88, 2105–2111. https://doi.org/10.1590/0001-3765201620140641.

Aragón-Moreno, A.A., Islebe, G.A., Torrescano-Valle, N., Arellano-Verdejo, J., 2018. Middle and late Holocene mangrove dynamics of the Yucatan Peninsula, Mexico. J. South Am. Earth Sci. 85, 307–311. https://doi.org/10.1016/j.jsames.2018.05.015.

Beebower, J.R., 1964. Cyclothems and cyclic depositional mechanism in alluvial plain sedimentation. Bull. Kans. Univ. Geol. Surv. 169, 35–42.

Behling, H., Cohen, M.C.L., Lara, R.J., 2001. Studies on Holocene mangrove ecosystem dynamics of the Bragança Peninsula in north-eastern Pará, Brazil. Bosque 167, 225–242.

Behling, H., Cohen, M.L., Lara, R., 2004. Late Holocene mangrove dynamics of Marajó Island in Amazonia, northern Brazil. Veg. Hist. Archaeobot. 13, 73–80. https://doi.org/10.1007/s00334-004-0031-1.

Benson, A., 2010. *Rangia cuneata*. USGS Nonindigenous Aquatic Species Database, Gainesville, FL. [online] Available from. https://www.fws.gov/fisheries/ans/erss/uncertainrisk/Rangia-cuneata-WEB-10-01-12.pdf. (Accessed 12 April 2020).

Blasco, F., 1996. Mangroves as indicators of coastal change. Catena 27, 167–178.

Blasco, F., Saenger, P., Janodet, E., 1996. Mangroves as indicators of coastal change. CATENA 27, 167–178. https://doi.org/10.1016/0341-8162(96)00013-6.

Blum, M.D., Roberts, H.H., 2012. The Mississippi Delta Region: past, present, and future. Annu. Rev. Earth Planet. Sci. 40, 655–683. https://doi.org/10.1146/annurev-earth-042711-105248.

Blum, M.D., Carter, A.E., Zayac, T., Goble, R., 2002. Middle Holocene sea-level and evolution of the Gulf of Mexico Coast (USA). J. Coast. Res. 36, 65–80. https://doi.org/10.2112/1551-5036-36.sp1.65.

Braconnot, P., Otto-Bliesner, B., Harrison, S., Joussaume, S., Peterchmitt, J.Y., Abe-Ouchi, A., Crucifix, M., Driesschaert, E., Fichefet, T., Hewitt, C.D., Kageyama, M., Kitoh, A., Laîné, A., Loutre, M.F., Marti, O., Merkel, U., Ramstein, G., Valdes, P., Weber, S.L., Yu, Y., Zhao, Y., 2007. Results of PMIP2 coupled simulations of the Mid-Holocene and last glacial maximum - part 1: experiments and large-scale features. Clim. Past 3, 261–277. https://doi.org/10.5194/cp-3-261-2007.

Bradley, R.S., Jones, P.D., 1992. When was the "Little Ice Age"? In: Mikami, T. (Ed.), Proceedings of the International Symposium on the "Little Ice Age" Climate. Department of Geography, Tokyo Metropolitan University, pp. 1–4

Brantley, S.T., Bissett, S.N., Young, D.R., Wolner, C.W.V., Moore, L.J., 2014. Barrier Island morphology and sediment characteristics affect the recovery of dune building grasses following storm-induced overwash. PLoS One 9, e104747. https://doi.org/10.1371/journal.pone.0104747.

Broecker, W.S., Stocker, T.F., 2006. The Holocene CO_2 rise: anthropogenic or natural? Eos (Washington. DC) 87, 27. https://doi.org/10.1029/2006EO030002.

Brush, G.S., Brush, L.M., 1972. Transport of pollen in a sediment-laden channel; a laboratory study. Am. J. Sci. 272, 359–381. https://doi.org/10.2475/ajs.272.4.359.

Buso Junior, A.A., Pessenda, L.C.R., Oliveira, P.E., Giannini, P.C., Cohen, M.C.L., Volkmer-Ribeiro, C., Barros de Oliveira, S.M., Favaro, D.I.T., Rossetti, D.F., Lorente, F., Borotti Filho, M.A., Schiavo, J.A., Bendassolli, J.A., França, M.C., Guimaraes, J.F., Siqueira, G., 2013. From an estuary to a freshwater lake: a paleo-estuary evolution in the context of Holocene sea-level fluctuations, Southeastern Brazil. Radiocarbon 55, 1735–1746. https://doi.org/10.2458/azu_js_rc.55.16210.

Caballero, M., Peinalba, M.C., Martinez, M., Ortega-Guerrerol, B., Vazquez, L., 2005. A Holocene record from a former coastal lagoon in Bahia Kino, Gulf of California, Mexico. The Holocene 15, 1236–1244. https://doi.org/10.1191/0959683605hl896rr.

Caldas, L.H. de O., Oliveira, J.G. de M., Stattegger, W.E. de, Stattegger, K., Vital, H., 2006. Geometry and evolution of Holocene transgressive and regressive barriers on the semi-arid coast of NE Brazil. Geo-Mar. Lett. 26, 249–263. https://doi.org/10.1007/s00367-006-0034-2.

Cannon, C.H., Morley, R.J., Bush, A.B.G., 2009. The current refugial rainforests of Sundaland are unrepresentative of their biogeographic past and highly vulnerable to disturbance. Proc. Natl. Acad. Sci. U. S. A. 106, 11188–11193. https://doi.org/10.1073/pnas.0809865106.

Cavanaugh, K.C., Kellner, J.R., Forde, A.J., Gruner, D.S., Parker, J.D., Rodriguez, W., Feller, I.C., 2014. Poleward expansion of mangroves is a threshold response to decreased frequency of extreme cold events. Proc. Natl. Acad. Sci. 111, 723–727. https://doi.org/10.1073/pnas.1315800111.

Cavanaugh, K.C., Parker, J.D., Cook-Patton, S.C., Feller, I.C., Williams, A.P., Kellner, J.R., 2015. Integrating physiological threshold experiments with climate modeling to project mangrove species' range expansion. Glob. Chang. Biol. 21, 1928–1938. https://doi.org/10.1111/gcb.12843.

Cavanaugh, K.C., Osland, M.J., Bardou, R., Hinojosa-Arango, G., López-Vivas, J.M., Parker, J.D., Rovai, A.S., 2018. Sensitivity of mangrove range limits to climate variability. Glob. Ecol. Biogeogr. 27, 925–935. https://doi.org/10.1111/geb.12751.

Cavanaugh, K.C., Dangremond, E.M., Doughty, C.L., Park Williams, A., Parker, J.D., Hayes, M.A., Rodriguez, W., Feller, I.C., 2019. Climate-driven regime shifts in a mangrove–salt marsh ecotone over the past 250 years. Proc. Natl. Acad. Sci. U. S. A. 116, 21602–21608. https://doi.org/10.1073/pnas.1902181116.

Cecil, C.B., 2013. An overview and interpretation of autocyclic and allocyclic processes and the accumulation of strata during the Pennsylvanian–Permian transition in the central Appalachian Basin, USA. Int. J. Coal Geol. 119, 21–31. https://doi.org/10.1016/j.coal.2013.07.012.

Chapman, V.J., 1975. Mangrove biogeography. In: Walsh, G.E., Snedaker, S.C., Teas, H.J. (Eds.), International Symposium on Biology and Management of Mangroves. University of Florida Press, Miami, pp. 179–212.

Clark, P.U., Dyke, A.S., Shakun, J.D., Carlson, A.E., Clark, J., Wohlfarth, B., Mitrovica, J.X., Hostetler, S.W., McCabe, A.M., 2009. The Last Glacial Maximum. Science 325, 710–714. https://doi.org/10.1126/science.1172873.

Coastal Engineering Consultants, 2015. Caminada headland beach and dune restoration (BA-45) completion report; Coastal protection and restoration authority. Baton Rouge, LA, USA.

Cohen, M.C.L., Behling, H., Lara, R.J., 2005a. Amazonian mangrove dynamics during the last millennium: the relative sea-level and the Little Ice Age. Rev. Palaeobot. Palynol. 136, 93–108. https://doi.org/10.1016/j.revpalbo.2005.05.002.

Cohen, M.C.L., Souza Filho, P.W.M., Lara, R.J., Behling, H., Angulo, R.J., 2005b. A model of Holocene mangrove development and relative sea-level changes on the Bragança Peninsula (northern Brazil). Wetl. Ecol. Manag. 13, 433–443. https://doi.org/10.1007/s11273-004-0413-2.

Cohen, M.C.L., Lara, R.J., Smith, C.B., Angélica, R.S., Dias, B.S., Pequeno, T., 2008. Wetland dynamics of Marajó Island, northern Brazil, during the last 1000 years. CATENA 76, 70–77.

Cohen, M.C.L., Behling, H., Lara, R.J., Smith, C.B., Matos, H.R.S., Vedel, V., 2009. Impact of sea-level and climatic changes on the Amazon coastal wetlands during the late Holocene. Veg. Hist. Archaeobot. 18, 425–439. https://doi.org/10.1007/s00334-008-0208-0.

Cohen, M.C.L., Pessenda, L.C.R., Behling, H., de Fátima Rossetti, D., França, M.C., Guimarães, J.T.F., Friaes, Y., Smith, C.B., 2012. Holocene palaeoenvironmental history of the Amazonian mangrove belt. Quat. Sci. Rev. 55, 50–58.

Cohen, M.C.L., França, M.C., Rossetti, D., Pessenda, L.C.R., Giannini, P.C.F., Lorente, F.L., Junior, A.Á.B., Castro, D., Macario, K., 2014a. Landscape evolution during the late Quaternary at the Doce River mouth, Espírito Santo State, Southeastern Brazil. Palaeogeogr. Palaeoclimatol. Palaeoecol. 415, 48–58. https://doi.org/10.1016/j.palaeo.2013.12.001.

Cohen, M.C.L., Pessenda, L.C.R., Smith, C.B., Guimarães, J.T.F., França, M.C., 2014b. Amazonian mangroves during the Late Pleistocene and Holocene. In: Carvalho, I. de S., Garcia, M., Lana, C.C., Strohschoen, O. (Eds.), Paleontologia: Cenários de Vida - Paleoclimas. Interciência, Rio de Janeiro, pp. 387–402.

Cohen, M.C.L., Rossetti, D.F., Pessenda, L.C.R., Friaes, Y.S., Oliveira, P.E., 2014c. Late Pleistocene glacial forest of Humaitá-Western Amazonia. Palaeogeogr. Palaeoclimatol. Palaeoecol. 415, 37–47. https://doi.org/10.1016/j.palaeo.2013.12.025.

Cohen, M.C.L., Alves, I.C.C., França, M.C., Pessenda, L.C.R., Rossetti, D. de F., 2015. Relative sea-level and climatic changes in the Amazon littoral during the last 500 years. CATENA 133, 441–451. https://doi.org/10.1016/j.catena.2015.06.012.

Cohen, M.C.L., Lara, R.J., Cuevas, E., Oliveras, E.M., Da Silveira Sternberg, L., 2016. Effects of sea-level rise and climatic changes on mangroves from southwestern littoral of Puerto Rico during the middle and late Holocene. Catena 143. https://doi.org/10.1016/j.catena.2016.03.041.

Cohen, M.C.L., Figueiredo, B.L., Oliveira, N.N., Fontes, N.A., França, M.C., Pessenda, L.C.R., de Souza, A.V., Macario, K., Giannini, P.C.F., Bendassolli, J.A., Lima, P., 2020a. Impacts of Holocene and modern sea-level changes on estuarine mangroves from northeastern Brazil. Earth Surf. Process. Landforms 45, 375–392. https://doi.org/10.1002/esp.4737.

Cohen, M.C.L., Rodrigues, E., Rocha, D.O.S., Freitas, J., Fontes, N.A., Pessenda, L.C.R., de Souza, A.V., Gomes, V.L.P., França, M.C., Bonotto, D.M., Bendassolli, J.A., 2020b. Southward migration of the austral limit of mangroves in South America. Catena 195, 104775. https://doi.org/10.1016/j.catena.2020.104775.

Cordero-Oviedo, C., Correa-Metrio, A., Urrego, L.E., Vázquez, G., Blaauw, M., Escobar, J., Curtis, J.H., 2019. Holocene establishment of mangrove forests in the western coast of the Gulf of Mexico. Catena 180, 212–223. https://doi.org/10.1016/j.catena.2019.04.025.

Cuven, S., Paris, R., Falvard, S., Miot-Noirault, E., Benbakkar, M., Schneider, J.L., Billy, I., 2013. High-resolution analysis of a tsunami deposit: case-study from the 1755 Lisbon tsunami in southwestern Spain. Mar. Geol. 337, 98–111. https://doi.org/10.1016/j.margeo.2013.02.002.

Davis, M.B., 2000. Palynology after Y2K — understanding the source area of pollen in sediments. Annu. Rev. Earth Planet. Sci. 28, 1–18.

Deines, P., 1980. The isotopic composition of reduced organic carbon. In: Fritz, P., Fontes, J.C. (Eds.), Handbook of Environmental Isotope Geochemistry. The Terrestrial Environments. Elsevier, Amsterdam, pp. 329–406.

Dietz, M., Liu, K., Bianchette, T., Dietz, M.E., Liu, K., Bianchette, T.A., 2018. Hurricanes as a major driver of coastal erosion in the Mississippi River Delta: a multi-decadal analysis of shoreline retreat rates at Bay Champagne, Louisiana (USA). Water 10, 1480. https://doi.org/10.3390/w10101480.

Dittmar, T., Hertkorn, N., Kattner, G., Lara, R.J., 2006. Mangroves, a major source of dissolved organic carbon to the oceans. Glob. Biogeochem. Cycles 20. https://doi.org/10.1029/2005GB002570 n/a-n/a.

Donnelly, C., Kraus, N., Larson, M., 2006. State of knowledge on measurement and modeling of coastal overwash. J. Coast. Res. 22, 965–991. https://doi.org/10.2112/04-0431.1.

Donoghue, J.F., 2011. Sea level history of the northern Gulf of Mexico coast and sea level rise scenarios for the near future. Clim. Chang. 107, 17–33. https://doi.org/10.1007/s10584-011-0077-x.

Duke, N.C., 1992. Mangrove floristics and biogeography. American Geophysical Union (AGU), pp. 63–100 https://doi.org/10.1029/CE041p0063.

Duke, N.C., Ball, M.C., Ellison, J.C., 1998. Factors influencing biodiversity and distributional gradients in mangroves. Glob. Ecol. Biogeogr. Lett. 7, 27–47. https://doi.org/10.2307/2997695.

Everitt, J.H., Judd, F.W., Escobar, D.E., Davis, M.R., 1996. Integration of remote sensing and spatial information technologies for mapping black mangrove on the Texas gulf coast. J. Coast. Res. 12, 64–69.

Ewel, K.C., Twilley, R.R., Ong, J.E., 1998. Different kinds of mangrove forests provide different goods and services. Glob. Ecol. Biogeogr. Lett. 7, 83–94.

Faegri, K., Iversen, J., 1989. Textbook of Pollen Analyses. John Wiley and Sons, New York 328 p.

Finkelstein, S.A., 2003. Identifying pollen grains of *Typha latifolia*, *Typha angustifolia*, and Typha xglauca. Can. J. Bot. 81, 985–990. https://doi.org/10.1139/b03-084.

Fisher, R., Huo, J., 2012. A Business Plan for Blue Carbon Offsets at Duke University (Master of Environmental Management degree in the Nicholas School of the Environment of Duke University).

Fontes, N.A., Moraes, C.A., Cohen, M.C.L., Alves, I.C.C., França, M.C., Pessenda, L.C.R., Francisquini, M.I., Bendassolli, J.A., Macario, K., Mayle, F., 2017. The impacts of the Middle Holocene high sea-level stand and climatic changes on mangroves of the Jucuruçu River, Southern Bahia – Northeastern Brazil. Radiocarbon 59, 215–230. https://doi.org/10.1017/RDC.2017.6.

Food and Agriculture Organization of the United Nations, 2007. The World's Mangroves, 1980–2005: A Thematic Study in the Framework of the Global Forest Resources Assessment 2005. Food and Agriculture Organization of the United Nations.

França, M.C., Cohen, M.C.L., Pessenda, L.C.R., Rossetti, D.F., Lorente, F.L., Buso Junior, A.Á., Guimarães, J.T.F., Friaes, Y., Macario, K., 2013. Mangrove vegetation changes on Holocene terraces of the Doce River, southeastern Brazil. Catena 110, 59–69.

França, M.C., Francisquini, M.I., Cohen, M.C.L., Pessenda, L.C.R., 2014. Inter-proxy evidence for the development of the Amazonian mangroves during the Holocene. Veg. Hist. Archaeobot. 23, 527–542. https://doi.org/10.1007/s00334-013-0420-4.

França, M.C., Alves, I.C.C., Castro, D.F., Cohen, M.C.L., Rossetti, D.F., Pessenda, L.C.R., Lorente, F.L., Fontes, N.A., Junior, A.Á.B., Giannini, P.C.F., Francisquini, M.I., 2015. A multi-proxy evidence for the transition from estuarine mangroves to deltaic freshwater marshes, Southeastern Brazil, due to climatic and sea-level changes during the late Holocene. Catena 128, 155–166. https://doi.org/10.1016/j.catena.2015.02.005.

França, M.C., Alves, I.C.C., Cohen, M.C., Rossetti, D.F., Pessenda, L.C., Giannini, P.C., Lorente, F.L., Buso Junior, A.A., Bendassolli, J.A., Macario, K., 2016. Millennial to secular timescale impacts of climate and sea-level changes on mangroves from the Doce River delta, Southeastern Brazil. The Holocene 26, 1733–1749. https://doi.org/10.1177/0959683616645938.

França, M.C., Pessenda, L.C., Cohen, M.C., de Azevedo, A.Q., Fontes, N.A., Silva, F.B., de Melo, J.C., Piccolo, M. de C., Bendassolli, J.A., Macario, K., 2019. Late-Holocene subtropical mangrove dynamics in response to climate change during the last millennium. The Holocene 29, 445–456. https://doi.org/10.1177/0959683616816438.

Fromard, F., Vega, C., Proisy, C., 2004. Half a century of dynamic coastal change affecting mangrove shorelines of French Guiana. A case study based on remote sensing data analyses and field surveys. Mar. Geol. 208, 265–280. https://doi.org/10.1016/j.margeo.2004.04.018.

Giri, C., Ochieng, E., Tieszen, L.L., Zhu, Z., Singh, A., Loveland, T., Masek, J., Duke, N., 2011. Status and distribution of mangrove forests of the world using earth observation satellite data. Glob. Ecol. Biogeogr. 20, 154–159. https://doi.org/10.1111/j.1466-8238.2010.00584.x.

Gischler, E., 2015. Quaternary reef response to sea-level and environmental change in the western Atlantic. Sedimentology 62, 429–465. https://doi.org/10.1111/sed.12174.

Gosling, W.D., Mayle, F.E., Tate, N.J., Killeen, T.J., 2009. Differentiation between Neotropical rainforest, dry forest, and savannah ecosystems by their modern pollen spectra and implications for the fossil pollen record. Rev. Palaeobot. Palynol. 153, 70–85. https://doi.org/10.1016/j.revpalbo.2008.06.007.

Grimm, E., 1990. TILIA and TILIAGRAPH: PC spreadsheet and graphic software for pollen data. INQUA Sub-Commission on Data-Handling Methods Newsletter.

Guimarães, J.T.F., Cohen, M.C.L., Pessenda, L.C.R., Franca, M.C., Smith, C.B., Nogueira, A.C.R., 2011. Mid- and late-Holocene sedimentary process and palaeovegetation changes near the mouth of the Amazon River. The Holocene 22, 359–370. https://doi.org/10.1177/0959683611423693.

Guimarães, J.T.F., Cohen, M.C.L., Franca, M.C., Pessenda, L.C.R., Behling, H., 2013. Morphological and vegetation changes on tidal flats of the Amazon Coast during the last 5000 cal. yr BP. The Holocene 23, 528–543. https://doi.org/10.1177/0959683612463097.

Hamdi, S.M.M., Assadi, M., Segarra-Moragues, J.G., 2010. Pollen morphology of Iranian species of Typha L. (Typhaceae) and its taxonomic significance. Feddes Repert. 121, 85–96. https://doi.org/10.1002/fedr.200911130.

Hameed, M., Nawaz, T., Ashraf, M., Tufail, A., Kanwal, H., Sajid Aqeel Ahmad, M., Ahmad, I., 2012. Leaf Anatomical Adaptations of Some Halophytic and Xerophytic Sedges of the Punjab.

Harper, C., 1984. Improved methods of facies sequence analysis. Facies Model.

Harris, M.S., Sautter, L.R., Johnson, K.L., Luciano, K.E., Sedberry, G.R., Wright, E.E., Siuda, A.N.S., 2013. Continental shelf landscapes of the southeastern United States since the last interglacial. Geomorphology 203, 6–24. https://doi.org/10.1016/j.geomorph.2013.02.014.

Havinga, A.J., 1967. Palynology and pollen preservation. Rev. Paleobot. Palynol. 2, 81–98.

Henry, K.M., Twilley, R.R., 2013. Soil development in a coastal Louisiana wetland during a climate-induced vegetation shift from salt marsh to mangrove. J. Coast. Res. 292, 1273–1283. https://doi.org/10.2112/JCOASTRES-D-12-00184.1.

IPCC, 2014. Contribution of working groups I, II and III to the fifth assessment report of the intergovernmental panel on climate change. In: Pachauri, R.K., Meyer, L.A. (Eds.), Climate Change 2014: Synthesis Report. Geneva, p. 151.

Jafari, N.H., Harris, B.D., Stark, T.D., 2018. Geotechnical investigations at the caminada headlands beach and dune in coastal Louisiana. Coast. Eng. 142, 82–94. https://doi.org/10.1016/j.coastaleng.2018.04.014.

Joe-Wong, C., Schlesinger, D.R., Chow, A.T., Myneni, S.C.B., 2019. Sea level rise produces abundant organobromines in salt-affected coastal wetlands. Geochem. Persp. Lett. 10, 31–35. https://doi.org/10.7185/geochemlet.1911.

Johnson, C.L., Chen, Q., Ozdemir, C.E., 2020. Lidar time-series analysis of a rapidly transgressing low-lying mainland barrier (Caminada Headlands, Louisiana, USA). Geomorphology 352, 106979. https://doi.org/10.1016/j.geomorph.2019.106979.

Jomelli, V., Khodri, M., Favier, V., Brunstein, D., Ledru, M.-P., Wagnon, P., Blard, P.-H., Sicart, J.-E., Braucher, R., Grancher, D., Bourlè, L., Braconnot, P., Vuille, M., 2011. Irregular tropical glacier retreat over the Holocene epoch driven by92nprogressive warming. Nature. https://doi.org/10.1038/nature10150.

Jones, M.C., Wingard, G.L., Stackhouse, B., Keller, K., Willard, D., Marot, M., Landacre, B.E., Bernhardt, C., 2019. Rapid inundation of southern Florida coastline despite low relative sea-level rise rates during the late-Holocene. Nat. Commun. 10, 1–13. https://doi.org/10.1038/s41467-019-11138-4.

Kaplan, J.O., Krumhardt, K.M., Ellis, E.C., Ruddiman, W.F., Lemmen, C., Goldewijk, K.K., 2011. Holocene carbon emissions as a result of anthropogenic land cover change. Holocene 21, 775–791. https://doi.org/10.1177/0959683610386983.

Kaufman, D., McKay, N., Routson, C., Erb, M., Davis, B., Heiri, O., Jaccard, S., Tierney, J., Dätwyler, C., Axford, Y., Brussel, T., Cartapanis, O., Chase, B., Dawson, A., de Vernal, A., Engels, S., Jonkers, L., Marsicek, J., Moffa-Sánchez, P., Morrill, C., Orsi, A., Rehfeld, K., Saunders, K., Sommer, P.S., Thomas, E., Tonello, M., Tóth, M., Vachula, R., Andreev, A., Bertrand, S., Biskaborn, B., Bringué, M., Brooks, S., Caniupán, M., Chevalier, M., Cwynar, L., Emile-Geay, J., Fegyveresi, J., Feurdean, A., Finsinger, W., Fortin, M.C., Foster, L., Fox, M., Gajewski, K., Grosjean, M., Hausmann, S., Heinrichs, M., Holmes, N., Ilyashuk, B., Ilyashuk, E., Juggins, S., Khider, D., Koinig, K., Langdon, P., Larocque-Tobler, I., Li, J., Lotter, A., Luoto, T., Mackay, A., Magyari, E., Malevich, S., Mark, B., Massaferro, J., Montade, V., Nazarova, L., Novenko, E., Pařil, P., Pearson, E., Peros, M., Pienitz, R., Płóciennik, M., Porinchu, D., Potito, A., Rees, A., Reinemann, S., Roberts, S., Rolland, N., Salonen, S., Self, A., Seppä, H., Shala, S., St-Jacques, J.M., Stenni, B., Syrykh, L., Tarrats, P., Taylor, K., van den Bos, V., Velle, G., Wahl, E., Walker, I., Wilmshurst, J., Zhang, E., Zhilich, S., 2020. A global database of Holocene paleotemperature records. Sci. Data 7, 1–34. https://doi.org/10.1038/s41597-020-0445-3.

Kennedy, J.P., Pil, M.W., Proffitt, C.E., Boeger, W.A., Stanford, A.M., Devlin, D.J., 2016. Postglacial expansion pathways of red mangrove, *Rhizophora mangle*, in the Caribbean Basin and Florida. Am. J. Bot. 103, 260–276. https://doi.org/10.3732/ajb.1500183.

Khan, N.S., Ashe, E., Horton, B.P., Dutton, A., Kopp, R.E., Brocard, G., Engelhart, S.E., Hill, D.F., Peltier, W.R., Vane, C.H., Scatena, F.N., 2017. Drivers of Holocene sea-level change in the Caribbean. Quat. Sci. Rev. https://doi.org/10.1016/j.quascirev.2016.08.032.

Kjerfve, B., 1994. Coastal Lagoons. Elsevier Oceanogr. Ser. 60, pp. 1–8. https://doi.org/10.1016/S0422-9894(08)70006-0.

Krauss, K.W., McKee, K.L., Lovelock, C.E., Cahoon, D.R., Saintilan, N., Reef, R., Chen, L., 2014. How mangrove forests adjust to rising sea level. New Phytol. 202, 19–34. https://doi.org/10.1111/nph.12605.

Kulp, M., Penland, S., Williams, S.J., Jenkins, C., Flocks, J., Kindinger, J., 2005. Geologic framework, evolution, and sediment resources for restoration of the Louisiana coastal zone. J. Coast. Res. https://doi.org/10.2307/25737049.

Ladislas, S., El-Mufleh, A., Gérente, C., Chazarenc, F., Andrès, Y., Béchet, B., 2012. Potential of aquatic macrophytes as bioindicators of heavy metal pollution in urban stormwater runoff. Water Air Soil Pollut. 223, 877–888. https://doi.org/10.1007/s11270-011-0909-3.

Lara, R.J., Cohen, M.C.L., 2006. Sediment porewater salinity, inundation frequency and mangrove vegetation height in Bragança, North Brazil: an ecohydrology-based empirical model. Wetl. Ecol. Manag. 14, 349–358. https://doi.org/10.1007/s11273-005-4991-4.

Lara, R.J., Cohen, M.C.L., 2009. Palaeolimnological studies and ancient maps confirm secular climate fluctuations in Amazonia. Clim. Chang. 94, 399–408. https://doi.org/10.1007/s10584-008-9507-9.

Lean, J., Rind, D., 1999. Evaluating sun-climate relationships since the Little Ice Ag. J. Atmos. Solar Terrest. Phys. 61, 25–36.

Lima, W.J.S., Cohen, M.C.L., Rossetti, D.F., França, M.C., 2017. Late Pleistocene glacial forest elements of Brazilian Amazonia. Palaeogeogr. Palaeoclimatol. Palaeoecol. https://doi.org/10.1016/j.palaeo.2017.11.050.
Liu, K., 2004. Paleotempestology: principles, methods, and examples from Gulf coast lake-sediments. In: Murnane, R., Liu, K.B. (Eds.), Hurricanes and Typhoons: Past, Present, and Future. Columbia University, New York, pp. 13–57.
Liu, K., Li, C., Bianchette, T., McCloskey, T., 2011. Storm deposition in a coastal backbarrier lake in Louisiana caused by hurricanes Gustav and Ike. J. Coast. Res. 64, 1866–1870.
Liu, Z., Zhu, J., Rosenthal, Y., Zhang, X., Otto-Bliesner, B.L., Timmermann, A., Smith, R.S., Lohmann, G., Zheng, W., Timm, O.E., 2014. The Holocene temperature conundrum. Proc. Natl. Acad. Sci. U. S. A. 111, E3501–E3505. https://doi.org/10.1073/pnas.1407229111.
Lloyd, F.E., Tracy, S.M., 1901. The insular flora of Mississippi and Louisiana. Bull. Torrey Bot. Club 28, 61. https://doi.org/10.2307/2477884.
Lohmann, G., Pfeiffer, M., Laepple, T., Leduc, G., Kim, J.H., 2013. A model-data comparison of the Holocene global sea surface temperature evolution. Clim. Past 9, 1807–1839. https://doi.org/10.5194/cp-9-1807-2013.
Lorente, F.L., Pessenda, L.C.R., Oboh-Ikuenobe, F., Buso Jr., A.A., Cohen, M.C.L., Meyer, K.E.B., Giannini, P.C.F., de Oliveira, P.E., Rossetti, D. de F., Borotti Filho, M.A., França, M.C., de Castro, D.F., Bendassolli, J.A., Macario, K., 2013. Palynofacies and stable C and N isotopes of Holocene sediments from Lake Macuco (Linhares, Espírito Santo, southeastern Brazil): depositional settings and palaeonvironmental evolution. Palaeogeogr. Palaeoclimatol. Palaeoecol. 55, 325–330. https://doi.org/10.1016/j.palaeo.2013.12.004.
Lugo, A.E., Patterson-zucca, C., 1977. The Impact of Low Temperature Stress on Mangrove Structure and Growth.
Marcott, S.A., Shakun, J.D., Clark, P.U., Mix, A.C., 2013. A reconstruction of regional and global temperature for the past 11,300 years. Science 339 (80), 1198–1201. https://doi.org/10.1126/science.1228026.
McAndrews, J.H., McAndrews, J.H., Berti, A.A., Norris, G., Museum, R.O., 1973. Key to the Quaternary pollen and spores of the Great Lakes region. Royal Ontario Museum, Toronto 72 p.
McKee, K.L., Vervaeke, W.C., 2018. Will fluctuations in salt marsh–mangrove dominance alter vulnerability of a subtropical wetland to sea-level rise? Glob. Chang. Biol. 24, 1224–1238. https://doi.org/10.1111/gcb.13945.
McLeod, E., Salm, R.V., 2006. Managing Mangroves for Resilience to Climate Change. IUCN, Gland, Switzerland.
Meyer, H., Opel, T., Laepple, T., Dereviagin, A.Y., Hoffmann, K., Werner, M., 2015. Long-term winter warming trend in the Siberian Arctic during the mid- to late Holocene. Nat. Geosci. 8, 122–125. https://doi.org/10.1038/ngeo2349.
Meyers, Philip A., 1994. Preservation of elemental and isotopic source identification of sedimentary organic matter. Chem. Geol. 114, 289–302. https://doi.org/10.1016/0009-2541(94)90059-0.
Miall, A.D., 1978. Lithofacies types and vertical profile models in braided river deposits: a summary. Fluv. Sedimentol. 5, 597–600.
Mock, C.J., Mojzisek, J., McWaters, M., Chenoweth, M., Stahle, D.W., 2007. The winter of 1827–1828 over eastern North America: a season of extraordinary climatic anomalies, societal impacts, and false spring. Clim. Chang. 83, 87–115. https://doi.org/10.1007/s10584-006-9126-2.
Montoya, E., Pedra-Méndez, J., García-Falcó, E., Gómez-Paccard, M., Giralt, S., Vegas-Vilarrúbia, T., Stauffer, F.W., Rull, V., 2019. Long-term vegetation dynamics of a tropical megadelta: Mid-Holocene palaeoecology of the Orinoco Delta (NE Venezuela). Quat. Sci. Rev. https://doi.org/10.1016/j.quascirev.2019.105874.
Moraes, C.A., Fontes, N.A., Cohen, M.C., França, M.C., Pessenda, L.C., Rossetti, D.F., Francisquini, M.I., Bendassolli, J.A., Macario, K., 2017. Late Holocene mangrove dynamics dominated by autogenic processes. Earth Surf. Process. Landforms. https://doi.org/10.1002/esp.4167.
Mulvaney, R., Abram, N.J., Hindmarsh, R.C.A., Arrowsmith, C., Fleet, L., Triest, J., Sime, L.C., Alemany, O., Foord, S., 2012. Recent Antarctic Peninsula warming relative to Holocene climate and ice-shelf history. Nature 489, 141–144. https://doi.org/10.1038/nature11391.
Murray-Wallace, C.V., 2007. Eustatic sea-level changes since the last glaciation. In: Elias, S.A. (Ed.), Encyclopedia of Quaternary Science. Elsevier, Amsterdam, pp. 3034–3043.
Naquin, J.D., Liu, K., McCloskey, T.A., Bianchette, T.A., 2014. Storm deposition induced by hurricanes in a rapidly subsiding coastal zone. J. Coast. Res. 70, 308–313. https://doi.org/10.2112/si70-052.1.
National Climatic Data Center, 2018. NOAA Baseline Climatological Dataset - Monthly Weather Station Temperature and Precipitation Data. www.ncdc.noaa.gov.
Nielsen, S.H.H., Koç, N., Crosta, X., 2004. Holocene climate in the Atlantic sector of the Southern Ocean: controlled by insolation or oceanic circulation? Geology 32, 317–320. https://doi.org/10.1130/G20334.1.
Nittrouer, C.A., Kuehl, S.A., Figueiredo, G., Allison, M.A., K, I.I.C., Rine, J.M., Faria, T.L.E.C., Silveira, O.M., 1996. The Geological Record Preserved by Amazon Shelf Sedimentation. p. 16.
O'ishi, R., Abe-Ouchi, A., 2011. Polar amplification in the mid-Holocene derived from dynamical vegetation change with a GCM. Geophys. Res. Lett. 38. https://doi.org/10.1029/2011GL048001 n/a-n/a.
Osland, M.J., Feher, L.C., 2020. Winter climate change and the poleward range expansion of a tropical invasive tree (Brazilian pepper—Schinus terebinthifolius). Glob. Chang. Biol. 26, 607–615. https://doi.org/10.1111/gcb.14842.
Osland, M.J., Day, R.H., From, A.S., McCoy, M.L., McLeod, J.L., Kelleway, J.J., 2015. Life stage influences the resistance and resilience of black mangrove forests to winter climate extremes. Ecosphere 6, art160. https://doi.org/10.1890/ES15-00042.1.
Osland, M.J., Day, R.H., Hall, C.T., Brumfield, M.D., Dugas, J.L., Jones, W.R., 2017. Mangrove expansion and contraction at a poleward range limit: climate extremes and land-ocean temperature gradients. Ecology 98, 125–137. https://doi.org/10.1002/ecy.1625.
Osland, M.J., Feher, L.C., López-Portillo, J., Day, R.H., Suman, D.O., Guzmán Menéndez, J.M., Rivera-Monroy, V.H., 2018. Mangrove forests in a rapidly changing world: Global change impacts and conservation opportunities along the Gulf of Mexico coast. Estuar. Coast. Shelf Sci. 214, 120–140. https://doi.org/10.1016/j.ecss.2018.09.006.
Osland, M.J., Hartmann, A.M., Day, R.H., Ross, M.S., Hall, C.T., Feher, L.C., Vervaeke, W.C., 2019. Microclimate influences mangrove freeze damage: implications for range expansion in response to changing macroclimate. Estuar. Coasts 42, 1084–1096. https://doi.org/10.1007/s12237-019-00533-1.
Peros, M.C., Reinhardt, E.G., Davis, A.M., 2007. A 6000-year record of ecological and hydrological changes from Laguna de la Leche, north coastal Cuba. Quat. Res. 67, 69–82. https://doi.org/10.1016/j.yqres.2006.08.004.
Perry, C.L., Mendelssohn, I.A., 2009. Ecosystem effects of expanding populations of *Avicennia germinans* in a Louisiana salt marsh. Wetlands 29, 396–406. https://doi.org/10.1672/08-100.1.
Pessenda, L.C.R., Ribeiro, A.D.S., Gouveia, S.E.M., Aravena, R., Boulet, R., Bendassolli, J.A., 2004. Vegetation dynamics during the late Pleistocene in the Barreirinhas region, Maranhão State, northeastern Brazil, based on carbon isotopes in soil organic matter. Quat. Res. 62, 183–193. https://doi.org/10.1016/j.yqres.2004.06.003.
Pessenda, L.C.R., Gouveia, S.E.M., Ribeiro, A. de S., De Oliveira, P.E., Aravena, R., 2010. Late Pleistocene and Holocene vegetation changes in northeastern Brazil determined from carbon isotopes and charcoal records in soils. Palaeogeogr. Palaeoclimatol. Palaeoecol. 297, 597–608. https://doi.org/10.1016/j.palaeo.2010.09.008.
Pessenda, L.C.R., Vidotto, E., De Oliveira, P.E., Buso, A.A., Cohen, M.C.L., Rossetti, D. de F., Ricardi-Branco, F., Bendassolli, J.A., 2012. Late Quaternary vegetation and coastal environmental changes at Ilha do Cardoso mangrove, southeastern Brazil. Palaeogeogr. Palaeoclimatol. Palaeoecol. 363, 57–68.
Quisthoudt, K., Schmitz, N., Randin, C.F., Dahdouh-Guebas, F., Robert, E.M.R., Koedam, N., 2012. Temperature variation among mangrove latitudinal range limits worldwide. Trees Struct. Funct. 26, 1919–1931. https://doi.org/10.1007/s00468-012-0760-1.
Reading, H.G., 1996. Sedimentary Environments: Processes, Facies and Stratigraphy. 3a ed. Blackwell Science.
Reimer, P.J., Bard, E., Bayliss, A., Beck, J.W., Blackwell, P.G., Ramsey, C.B., Buck, C.E., Cheng, H., Edwards, R.L., Friedrich, M., Grootes, P.M., Guilderson, T.P., Haflidason, H., Hajdas, I., Hatté, C., Heaton, T.J., Hoffmann, D.L., Hogg, A.G., Hughen, K.A., Kaiser, K.F., Kromer, B., Manning, S.W., Niu, M., Reimer, R.W., Richards, D.A., Scott, E.M., Southon, J.R., Staff, R.A, Turney, C.S.M., van der Plicht, J., 2013. IntCal13 and Marine13 radiocarbon age calibration curves 0–50,000 years cal BP. Radiocarbon 55, 1869–1887. https://doi.org/10.2458/azu_js_rc.55.16947.
Reineck, H.E., Singh, I.B., 1980. Depositional Sedimentary Environments, With Reference to Terrigenous Clastics. Second edition. Depos. Sediment. Environ. With Ref. to Terrigenous Clastics Textbook. (Second Ed. (Textb.).
Ribeiro, S.R., Batista, E.J.L., Cohen, M.C., França, M.C., Pessenda, L.C., Fontes, N.A., Alves, I.C., Bendassolli, J.A., 2018. Allogenic and autogenic effects on mangrove dynamics from the Ceará Mirim River, north-eastern Brazil, during the middle and late Holocene. Earth Surf. Process. Landforms. https://doi.org/10.1002/esp.4342.
Ribeiro, R. de A., Rovai, A.S., Twilley, R.R., Castañeda-Moya, E., 2019. Spatial variability of mangrove primary productivity in the neotropics. Ecosphere 10. https://doi.org/10.1002/ecs2.2841.
Rodriguez, A.B., Anderson, J.B., Siringan, F.P., Taviani, M., 2004. Holocene evolution of the East Texas coast and inner continental shelf: along-strike variability in coastal retreat rates. J. Sediment. Res. 74, 405–421. https://doi.org/10.1306/092403740405.
Rossetti, D.F., Cohen, M.C.L., Bertani, T.C., Hayakawa, E.H., Paz, J.D.S., Castro, D.F., Friaes, Y., 2014. Late Quaternary fluvial terrace evolution in the main southern Amazonian tributary. Catena 116. https://doi.org/10.1016/j.catena.2013.11.021.
Ruddiman, W.F., 2003. The anthropogenic greenhouse era began thousands of years ago. Clim. Chang. https://doi.org/10.1023/B:CLIM.0000004577.17928.fa.
Ruddiman, W.F., Fuller, D.Q., Kutzbach, J.E., Tzedakis, P.C., Kaplan, J.O., Ellis, E.C., Vavrus, S. J., Roberts, C.N., Fyfe, R., He, F., Lemmen, C., Woodbridge, J., 2016. Late Holocene climate: natural or anthropogenic? Rev. Geophys. https://doi.org/10.1002/2015RG000503.
Ryu, J., 2020. Late Holocene Environmental Changes and Ecosystem Dynamics in Louisiana's Coastal Wetlands: A Multi-Site, Multi-Proxy Investigation. Louisiana State University.
Saintilan, N., Wilson, N.C., Rogers, K., Rajkaran, A., Krauss, K.W., 2014. Mangrove expansion and salt marsh decline at mangrove poleward limits. Glob. Chang. Biol. 20, 147–157. https://doi.org/10.1111/gcb.12341.
Sandoval-Castro, E., Muñiz-Salazar, R., Enríquez-Paredes, L.M., Riosmena-Rodríguez, R., Dodd, R.S., Tovilla-Hernández, C., Arredondo-García, M.C., 2012. Genetic population structure of red mangrove (*Rhizophora mangle* L.) along the northwestern coast of Mexico. Aquat. Bot. 99, 20–26. https://doi.org/10.1016/J.AQUABOT.2012.01.002.
Santos, T.P., Franco, D.R., Barbosa, C.F., Belem, A.L., Dokken, T., Albuquerque, A.L.S., 2013. Millennial- to centennial-scale changes in sea surface temperature in the tropical South Atlantic throughout the Holocene. Palaeogeogr. Palaeoclimatol. Palaeoecol. 392, 1–8. https://doi.org/10.1016/j.palaeo.2013.08.019.
Saucier, R.T., 1994. Geomorphology and Quaternary Geologic History of the Lower Mississippi Valley. volume 1. U. S. Army Corps of Engineers, Vicksburg ed.
Shea Penland, J.R.S., 1988. Barrier Island Erosion and Protection in Louisiana: A Coastal Geomorphological Perspective. p. 38.
Sherrod, C.L., McMillan, C., 1985. The distributional history and ecology of mangrove vegetation along the northern Gulf of Mexico coastal region. Contrib. Mar. Sci. 28, 129–140.
Silva, M.N.A., Cohen, M.C.L., Rossetti, D.F., Pessenda, L.C.R., 2018. Did sea-level changes affect the Brazilian Amazon Forest during the Holocene? Radiocarbon 60, 91–112. https://doi.org/10.1017/RDC.2017.62.
Skvarla, J.J., Larson, D.A., 1963. Nature of cohesion within pollen tetrads of *Typha latifolia*. Science (80-) 140, 173–175. https://doi.org/10.1126/science.140.3563.173.

Smith, C.B., Cohen, M.C.L., Pessenda, L.C.R., França, M.C., Guimarães, J.T.F., Rossetti, D. de F., Lara, R.J., 2011. Holocene coastal vegetation changes at the mouth of the Amazon River. Rev. Palaeobot. Palynol. 168, 21–30.
Smith, C.B., Cohen, M.C.L., Pessenda, L.C.R., França, M.C., Guimarães, J.T.F., 2012. Holocenic proxies of sedimentary organic matter and the evolution of Lake Arari-Amazon Region. Catena 90, 26–38.
Solomon, A.M., Blasing, T.J., Solomon, J.A., 1982. Interpretation of floodplain pollen in alluvial sediments from an Arid Region. Quat. Res. 18, 52–71.
Solomon, S., Qin, D., Manning, M., Chen, Z., Marquis, M., Averyl, K.B., Tignor, M., Miller, H.L., 2007. Climate Change 2007: The Physical Science Basis. Contribution of Working Group I to the Fourth Assessment Report of the Intergovernmental Panel on Climate Change. Cambridge University Press.
Stevens, P.W., Fox, S.L., Montague, C.L., 2006. The interplay between mangroves and saltmarshes at the transition between temperate and subtropical climate in Florida. Wetl. Ecol. Manag. 14, 435–444. https://doi.org/10.1007/s11273-006-0006-3.
Stokes, D.J., Healy, T.R., Cooke, P.J., 2010. Expansion dynamics of monospecific, temperate mangroves and sedimentation in two embayments of a barrier-enclosed lagoon, Tauranga Harbour, New Zealand. J. Coast. Res. 261, 113–122. https://doi.org/10.2112/08-1043.1.
Stuart, S.A., Choat, B., Martin, K.C., Holbrook, N.M., Ball, M.C., 2007. The role of freezing in setting the latitudinal limits of mangrove forests. New Phytol. 173, 576–583. https://doi.org/10.1111/j.1469-8137.2006.01938.x.
Sun, X., Li, X., 1999. A pollen record of the last 37 ka in deep sea core 17940 from the northern slope of the South China Sea. Mar. Geol. 156, 227–244. https://doi.org/10.1016/S0025-3227(98)00181-9.
Sundqvist, H.S., Kaufman, D.S., McKay, N.P., Balascio, N.L., Briner, J.P., Cwynar, L.C., Sejrup, H.P., Seppä, H., Subetto, D.A., Andrews, J.T., Axford, Y., Bakke, J., Birks, H.J.B., Brooks, S. J., De Vernal, A., Jennings, A.E., Ljungqvist, F.C., Rühland, K.M., Saenger, C., Smol, J.P., Viau, A.E., 2014. Arctic Holocene proxy climate database - new approaches to assessing geochronological accuracy and encoding climate variables. Clim. Past 10, 1605–1631. https://doi.org/10.5194/cp-10-1605-2014.
Taillardat, P., Friess, D.A., Lupascu, M., 2018. Mangrove blue carbon strategies for climate change mitigation are most effective at the national scale. Biol. Lett. 14, 20180251. https://doi.org/10.1098/rsbl.2018.0251.
Tarver, J., 1972. Occurrence, distribution, and density of Rangia cuneata in Lakes Pontchartrain and Maurepas, Louisiana, (Louisiana Wild Life and Fisheries Commission. Technical bulletin no. 1) [WWW Document]. URL https://www.amazon.com/Occurrence-distribution-Pontchartrain-Louisiana-Commission/dp/B0006CD1SA (accessed 5.18.20).
Timm, O., Timmermann, A., 2007. Simulation of the last 21,000 years using accelerated transient boundary conditions. J. Clim. 20, 4377–4401. https://doi.org/10.1175/JCLI4237.1.
Tomlinsom, P.B., 1986. The Botany of Mangroves. Cambridge University Press, Cambridge.
Toscano, M.A., Macintyre, I.G., 2003. Corrected western Atlantic sea-level curve for the last 11,000 years based on calibrated 14C dates from *Acropora palmata* framework and intertidal mangrove peat. Coral Reefs 22, 257–270. https://doi.org/10.1007/s00338-003-0315-4.
Tyson, R.V., 1995. Sedimentary Organic Matter: Organic Facies and Palynofacies. Chapman and Hall, London.
Vedel, V., Behling, H., Cohen, M., Lara, R., 2006. Holocene mangrove dynamics and sea-level changes in northern Brazil, inferences from the Taperebal core in northeastern Pará State. Veg. Hist. Archaeobot. 15, 115–123. https://doi.org/10.1007/s00334-005-0023-9.
Vega, A.J., 2012. Louisiana Weather and Climate - Louisiana State University Baton Rouge [WWW Document] (URL https://books.google.com.br/books?id=0wglj5alm9oC&printsec=frontcover&hl=pt-BR#v=onepage&q&f=false (accessed 5.17.20)).
Wakida-Kusunoki, A.T., MacKenzie, C.L., 2004. Rangia and marsh clams, *Rangia cuneata*, *R. flexuosa*, and *Polymesoda caroliniana*, in Eastern México: distribution, biology and ecology, and historical fisheries. Mar. Fish. Rev. 66, 13–20.
Walker, R.G., 1992. Facies, facies models and modern stratigrahic concepts. In: Walker, R.G., James, N.P. (Eds.), Facies Models - Response to Sea Level Change. Geological Association of Canada, Ontario, pp. 1–14.
Walsh, G.E., 1974. Mangroves: a review. In: Reinold, R.J., Queen, W.H. (Eds.), Ecology of Halophytes. Academic Press, New York, pp. 51–174.
Walsh, J., Nittrouer, C., 2004. Mangrove-bank sedimentation in a mesotidal environment with large sediment supply, Gulf of Papua. Mar. Geol. 208, 225–248. https://doi.org/10.1016/j.margeo.2004.04.010.
Wanless, H.R., Parkinson, R.W., Tedesco, L.P., 1994. Sea level control on stability of Everglades wetlands. In: Davis, S.M., Ogden, J.C. (Eds.), Everglades: The Ecosystem and Its Restoration. St. Lucie Press, pp. 199–222.
Warzocha, J., Szymanek, L., Witalis, B., Wodzinowski, T., 2016. The first report on the establishment and spread of the alien clam *Rangia cuneata* (Mactridae) in the Polish part of the Vistula Lagoon (southern Baltic). Oceanologia 58, 54–58. https://doi.org/10.1016/j.oceano.2015.10.001.
Weng, C., Bush, M.B., Silman, M.R., 2004. An analysis of modern pollen rain on an elevational gradient in southern Peru. J. Trop. Ecol. 20, 113–124. https://doi.org/10.1017/S0266467403001068.
Willard, D.A., Bernhardt, C.E., 2011. Impacts of past climate and sea level change on Everglades wetlands: placing a century of anthropogenic change into a late-Holocene context. Clim. Chang. 107, 59–80. https://doi.org/10.1007/s10584-011-0078-9.
Willard, D.A., Bernhardt, C.E., Weimer, L., Cooper, S.R., Gamez, D., Jensen, J., 2004. Atlas of pollen and spores of the Florida everglades. Palynology 28, 175–227.
Woodroffe, C.D., Grindrod, J., 1991. Mangrove biogeography: the role of quaternary environmental and sea-level change. J. Biogeogr. 18, 479–492. https://doi.org/10.2307/2845685.
Woodroffe, C.D., Thom, B.G., Chappell, J., 1985. Development of widespread mangrove swamps in mid-Holocene times in northern Australia. Nature 317, 711–713. https://doi.org/10.1038/317711a0.
Woodroffe, S.A., Long, A.J., Punwong, P., Selby, K., Bryant, C.L., Marchant, R., Bronk Ramsey, C., Buck, C.E., Burr, G.S., Edwards, R.L., Friedrich, M., Grootes, P.M., Guilderson, T.P., Hajdas, I., Heaton, T.J., Hogg, A.G., Hughen, K.A., Kaiser, K.F., Kromer, B., McCormac, F.G., Manning, S.W., Reimer, R.W., Richards, D.A., Southon, J.R., Talamo, S., Turney, C.S.M., van der Plicht, J., Weyhenmeyer, C.E., 2015. Radiocarbon dating of mangrove sediments to constrain Holocene relative sea-level change on Zanzibar in the southwest Indian Ocean. The Holocene 25, 820–831. https://doi.org/10.1177/0959683615571422.
Xu, Q., Tian, F., Bunting, M.J., Li, Y., Ding, W., Cao, X., He, Z., 2012. Pollen source areas of lakes with inflowing rivers: modern pollen influx data from Lake Baiyangdian, China. Quat. Sci. Rev. 37, 81–91. https://doi.org/10.1016/j.quascirev.2012.01.019.
Yao, Q., Liu, K., 2017. Dynamics of marsh-mangrove ecotone since the mid-Holocene: a palynological study of mangrove encroachment and sea level rise in the Shark River Estuary, Florida. PLoS One 12, e0173670. https://doi.org/10.1371/journal.pone.0173670.
Yao, Q., Liu, K., Platt, W.J., Rivera-Monroy, V.H., 2015. Palynological reconstruction of environmental changes in coastal wetlands of the Florida Everglades since the mid-Holocene. Quat. Res. 83, 449–458. https://doi.org/10.1016/j.yqres.2015.03.005.
Yao, Q., Liu, K., Ryu, J., 2018. Multi-proxy characterization of hurricanes Rita and Ike storm deposits in the Rockefeller Wildlife Refuge, Southwestern Louisiana. J. Coast. Res. 85, 841–845. https://doi.org/10.2112/si85-169.1.
Yao, Q., Liu, K. Biu, Aragón-Moreno, A.A., Rodrigues, E., Xu, Y.J., Lam, N.S., 2020. A 5200-year paleoecological and geochemical record of coastal environmental changes and shoreline fluctuations in southwestern Louisiana: implications for coastal sustainability. Geomorphology 365, 107284. https://doi.org/10.1016/j.geomorph.2020.107284.
Zalasiewicz, J., Waters, C.N., Williams, M., Summerhayes, C., 2018. The Anthropocene as a Geological Time Unit: A Guide to the Scientific Evidence and Current Debate. Cambridge University Press.